

# Evaluation of OMI operational standard NO<sub>2</sub> column retrievals using in situ and surface-based NO<sub>2</sub> observations

L. N. Lamsal<sup>1,2</sup>, N. A. Krotkov<sup>2</sup>, E. A. Celarier<sup>1,2</sup>, W. H. Swartz<sup>3,2</sup>, K. E. Pickering<sup>2</sup>, E. J. Bucsela<sup>4</sup>, J. F. Gleason<sup>2</sup>, R. V. Martin<sup>5,6</sup>, S. Philip<sup>5</sup>, H. Irie<sup>7</sup>, A. Cede<sup>8,2</sup>, J. Herman<sup>9,2</sup>, A. Weinheimer<sup>10</sup>, J. J. Szykman<sup>11</sup>, and T. N. Knepp<sup>12,13</sup>

<sup>1</sup>Goddard Earth Sciences Technology and Research, Universities Space Research Association, Columbia, MD 21046, USA

<sup>2</sup>NASA Goddard Space Flight Center, Greenbelt, MD 20771, USA

<sup>3</sup>Johns Hopkins University Applied Physics Laboratory, Laurel, MD 20723, USA

<sup>4</sup>SRI International, Menlo Park, CA 94025, USA

<sup>5</sup>Department of Physics and Atmospheric Science, Dalhousie University, Halifax, NS, B3H 3J5, Canada

<sup>6</sup>Also at Harvard-Smithsonian Center for Astrophysics, Cambridge, MA, USA

<sup>7</sup>Center for Environmental Remote Sensing, Chiba University, 1-33, Yayoicho, Inage-ku, Chiba 263-8522, Japan

<sup>8</sup>LuftBlick, Kreith, Austria

<sup>9</sup>University of Maryland, Joint Center for Earth Systems Technology, Baltimore, MD 21228, USA

<sup>10</sup>National Center for Atmospheric Research, Boulder, CO 80307, USA

<sup>11</sup>United States Environmental Protection Agency Office of Research and Development, Hampton, VA 23681, USA

<sup>12</sup>Science Systems and Applications, Inc., Hampton, VA 23681, USA

<sup>13</sup>NASA Langley Research Center, Hampton, VA 23681, USA

*Correspondence to:* L. N. Lamsal (lok.lamsal@nasa.gov)

## Abstract.

We assess the standard operational nitrogen dioxide (NO<sub>2</sub>) data product (OMNO2, version 2.1) retrieved from the Ozone Monitoring Instrument (OMI) onboard NASA's Aura satellite using a combination of aircraft and surface in situ measurements as well as ground-based column measurements at several locations and a bottom-up NO<sub>x</sub> emission inventory over the continental US. Despite considerable sampling differences, NO<sub>2</sub> vertical column densities from OMI are modestly correlated ( $r = 0.3\text{--}0.8$ ) with in situ measurements of tropospheric NO<sub>2</sub> from aircraft, ground-based observations of NO<sub>2</sub> columns from MAX-DOAS and Pandora instruments, in situ surface NO<sub>2</sub> measurements from photolytic converter instruments, and a bottom-up NO<sub>x</sub> emission inventory. Overall, OMI retrievals tend to be lower in urban regions and higher in remote areas, but generally agree with other measurements to within  $\pm 20\%$ . No consistent seasonal bias is evident. Contrasting results between different data sets reveal complexities behind NO<sub>2</sub> validation. Since validation data sets are scarce and are limited in space and time, validation of the global product is still limited in scope by

spatial and temporal coverage and retrieval conditions. Monthly mean vertical NO<sub>2</sub> profile shapes from the Global Modeling Initiative (GMI) chemistry-transport model (CTM) used in the OMI retrievals are highly consistent with in situ aircraft measurements, but these measured profiles exhibit considerable day-to-day variation, affecting the retrieved daily NO<sub>2</sub> columns by up to 40 %. This assessment of OMI tropospheric NO<sub>2</sub> columns, together with the comparison of OMI-retrieved and model-simulated NO<sub>2</sub> columns, could offer diagnostic evaluation of the model.

## 20 **1 Introduction**

Nitrogen oxides (NO<sub>x</sub>=NO+NO<sub>2</sub>) play a key role in atmospheric chemistry by controlling the production of tropospheric ozone, forming aerosol nitrates, and affecting the abundance of the hydroxyl radical (OH) and the lifetimes of greenhouse gases (Solomon et al., 1999; Intergovernmental Panel on Climate Change (IPCC), 2007). Nitrogen dioxide (NO<sub>2</sub>) is one of the pollutants regulated by the Environmental Protection Agency (EPA), as it is detrimental to human health and ecosystems (EPA, 2009). Major sources of NO<sub>x</sub> include combustion, soil emissions, and lighting. Tropospheric NO<sub>2</sub> concentrations are highly variable in space and time due to spatial heterogeneity of NO<sub>x</sub> sources and the relatively short lifetime of NO<sub>x</sub> in the lower troposphere.

NO<sub>2</sub> is measured locally by in situ monitors and detected remotely in an atmospheric column by ground-based and satellite instruments. NO<sub>2</sub> observations from satellite offer a globally consistent data set, albeit at coarse resolutions of 10 s to 100 s of kilometers, enabling a wide range of applications including many not feasible from in situ observations. Several studies have used satellite observations of NO<sub>2</sub> to evaluate chemical transport models (Martin et al., 2002; van Noije et al., 2006; Lamsal et al., 2008; Kim et al., 2009; Herron-Thorpe et al., 2010; Huijnen et al., 2010), examine spatial and temporal patterns of NO<sub>x</sub> emissions (Beirle et al., 2003; Richter et al., 2005; Kim et al., 2006; van der A et al., 2006; Zhang et al., 2007; Boersma et al., 2008a; Lu and Streets, 2012; Wang et al., 2012; Hilboll et al., 2013; Russell et al., 2010, 2012; Duncan et al., 2013), examine NO<sub>x</sub> sources (Jaeglé et al., 2005; van der A et al., 2008; Bucselá et al., 2010; de Wildt et al., 2012; Lin, 2012; Ghude et al., 2010, 2013a; Mebust et al., 2011; Mebust and Cohen, 2013), provide top-down constraints on surface NO<sub>x</sub> emissions (Martin et al., 2003; Konovalov et al., 2006; Zhao and Wang, 2009; Lin et al., 2010; Lamsal et al., 2011; Ghude et al., 2013b; Vinken et al., 2014), infer NO<sub>x</sub> lifetimes (Schaub et al., 2007; Lamsal et al., 2010; Beirle et al., 2011), and estimate surface NO<sub>2</sub> concentrations (Lamsal et al., 2008, 2013; Novotny et al., 2011; Bechle et al., 2013). The quality of the satellite data directly affects every one of these applications and estimates. Careful assessments of the accuracy of retrievals with credible, coincident, independent measurements help ensure reliable analyses.

Tropospheric NO<sub>2</sub> column retrievals from satellites have been evaluated with in situ NO<sub>2</sub> profile measurements from aircraft (Heland et al., 2002; Martin et al., 2006; Boersma et al., 2008a; Buc-

sela et al., 2008, 2013; Celarier et al., 2008; Hains et al., 2010), NO<sub>2</sub> column measurements from  
50 ground-based and airborne instruments (Ionov et al., 2008; Celarier et al., 2008; Brinkma et al.,  
2008; Kramer et al., 2008; Irie et al., 2008, 2012; Wenig et al., 2008; Oetjen et al., 2013), in situ  
surface measurements (Schaub et al., 2006; Blond et al., 2007; Boersma et al., 2009; Lamsal et al.,  
2008, 2010), and a bottom-up NO<sub>x</sub> emission inventory (Lamsal et al., 2010). Aircraft offer pre-  
55 cise in situ measurements within vertical spirals covering a spatial domain over a satellite field of  
view, but these are generally campaign-based experiments spanning only a few days to weeks and  
are limited by the need to extrapolate below the lowest measurement altitude (e.g. Bucselo et al.,  
2008). Ground-based NO<sub>2</sub> column observations from the Multi-AXis Differential Optical Absorp-  
tion Spectroscopy (MAX-DOAS) and direct-sun DOAS are maturing, but assessments with these  
60 measurements are still restricted by a limited number of sites. Validation with in situ surface NO<sub>2</sub>  
measurements from dense networks of commercial molybdenum converter analyzers are compli-  
cated by instrument interferents (e.g. Steinbacher et al., 2007; Lamsal et al., 2008), and is more  
appropriate in rural areas (Lamsal et al., 2010). Observations of NO<sub>2</sub> from photolytic converter ana-  
lyzers (Ryerson et al., 2000) are sparse, but offer useful opportunities to evaluate satellite retrievals.  
In the United States, the confidence in the estimates of local and regional emissions are at medium  
65 to high levels, suggesting low uncertainty in total continental NO<sub>x</sub> emissions (NARSTO, 2005).  
Validation using the US emission data benefits from a large domain coincident with satellite obser-  
vations and a variety of observational conditions. This study takes advantage of state-of-the-art NO<sub>2</sub>  
measurement techniques, and exploits the strength of various measurements to assess the quality of  
the new standard tropospheric NO<sub>2</sub> retrievals (OMNO2, version 2.1) from the Ozone Monitoring  
70 Instrument (OMI) under various atmospheric conditions.

Well-validated daily global observations from satellite provide a rich resource to evaluate results  
from regional air quality (AQ) models and global chemical transport models (CTMs), thereby help-  
ing to increase model accuracy. To facilitate satellite-model comparison, the OMNO2 product pro-  
vides information on vertical NO<sub>2</sub> measurement sensitivity (scattering weights). Combining scat-  
75 tering weights with model-derived vertical NO<sub>2</sub> profile shape allows for the calculation of new air  
mass factors (AMFs) needed to convert satellite-retrieved slant column densities (SCDs) to verti-  
cal column densities (VCDs). Since the assumed vertical distribution of NO<sub>2</sub> in the retrieval is  
taken from the model subject to evaluation, this approach allows consistent comparison of satellite-  
observed columns with model-simulated columns. Applying a similar approach for in situ NO<sub>2</sub>  
80 measurements from aircraft provides insights into the retrieval uncertainty, as using measured pro-  
files and resulting AMFs indicate how much the satellite retrieval would change when climatological  
assumptions about profile shape are replaced with specific, observed profile information.

Our main goals here are to assess the operational OMI NO<sub>2</sub> standard product, elucidate errors in  
retrieved columns due to a priori NO<sub>2</sub> vertical profiles through the use of nearly-coincident NO<sub>2</sub>  
85 profiles measured from aircraft, and devise objective methods to compare model-simulated NO<sub>2</sub>

columns with satellite retrievals. Section 2 describes the OMI retrievals and various concurrent data sources used in this study. We present validation results in Sect. 3. The impacts of the a priori NO<sub>2</sub> profiles used in the satellite retrievals are discussed in Sect. 4. We discuss the comparison of modeled and OMI NO<sub>2</sub> in Sect. 5. Section 6 summarizes the conclusions of this study.

## 90 2 Observations

### 2.1 OMI Retrieval

The Dutch-Finnish OMI instrument aboard the NASA EOS-Aura satellite provides continuous monitoring of atmospheric NO<sub>2</sub> columns through measurement of hyperspectral solar backscatter in the UV-visible range from 264 to 504 nm (Levelt et al., 2006). The satellite was launched on  
95 15 July 2004, into a polar, sun-synchronous orbit with an equator-crossing time of 13:45 LT (ascending node). OMI observes the atmosphere in 60 cross-track ground pixels measuring 13–26 km along track and 24–128 km across track, achieving daily global coverage.

We use the tropospheric NO<sub>2</sub> columns from OMI standard product (Bucsela et al., 2013) publicly available from the NASA archive: [http://disc.sci.gsfc.nasa.gov/Aura/data-holdings/OMI/omno2\\_v003.shtml](http://disc.sci.gsfc.nasa.gov/Aura/data-holdings/OMI/omno2_v003.shtml).  
100 shtml. The algorithm uses the Differential Absorption Spectroscopy (DOAS) technique (Platt, 1994) to determine NO<sub>2</sub> SCD by nonlinear least squares fitting of reference spectra for NO<sub>2</sub>, ozone, H<sub>2</sub>O and the Ring filling-in effect to the OMI-measured reflectance in the 405–465 nm spectral window (Bucsela et al., 2006; Boersma et al., 2007). The slant column represents the integrated NO<sub>2</sub> abundance along the average light path from the Sun, through the atmosphere, to the satellite. The  
105 measured SCDs are corrected for instrumental artifacts (stripes Dobber et al., 2008; Bucsela et al., 2013) accounting for cross-track variation of the stratospheric AMF. The AMF, defined as the ratio of the SCD to the VCD, is calculated using a look-up table of vertically resolved NO<sub>2</sub> sensitivities (scattering weights) and various input parameters including viewing geometry, surface reflectivity, effective cloud pressure, cloud radiance fraction, and a priori NO<sub>2</sub> vertical profile shapes (Palmer  
110 et al., 2001). The a priori NO<sub>2</sub> profiles are early afternoon (at the OMI overpass time) monthly mean values derived from the Global Modeling Initiative (GMI at 2° × 2.5°) CTM (Appendix A) (Strahan et al., 2007). To separate stratospheric and tropospheric columns, the algorithm first applies stratospheric (close to geometric) AMFs to the de-striped measured SCDs to yield initial VCDs. Cloud-free areas of tropospheric contamination in the stratospheric NO<sub>2</sub> field are identified using  
115 the a priori GMI monthly mean tropospheric NO<sub>2</sub> columns and OMI cloud measurements. Those regions are then masked and filled in with the stratospheric VCDs measured outside the masked regions, primarily from unpolluted or cloudy areas. The stratospheric field is further smoothed by using a boxcar averaging.

The OMNO2 retrievals used here, version 2.1 (Bucsela et al., 2013), represent a significant advance over previous version 1.0 (Bucsela et al., 2006; Celarier et al., 2008). The main changes  
120

include the use of monthly, rather than annual, mean a priori NO<sub>2</sub> profiles, and improvements in the estimates of stratospheric NO<sub>2</sub> columns, correction of calibration artifacts (de-stripping), and the calculation of scattering weights.

125 The uncertainties in the retrieval of tropospheric NO<sub>2</sub> columns arise from the uncertainties in the retrieval of slant column densities, the calculation of AMFs, and the separation of stratospheric and troposphere components. The uncertainty in the individual OMI NO<sub>2</sub> slant column is  $\sim 0.75 \times 10^{15}$  molec. cm<sup>-2</sup> (Boersma et al., 2004, 2011; Bucsela et al., 2013) and dominates the overall retrieval error over the oceans and remote areas. AMF uncertainties are  $\sim 20\%$  in clear-sky and 30–80% under cloudy conditions and dominate overall retrieval errors over continental polluted regions. In this study, we include the data for scenes with cloud radiance fractions less than 0.5 and those unaffected by the OMI row anomaly (Dobber et al., 2008). We use data from all cross-track positions.

## 2.2 In situ NO<sub>2</sub> measurements from aircraft

In situ NO<sub>2</sub> concentrations were measured from the NASA P-3B aircraft in the Baltimore-Washington, D.C. metropolitan region on 14 flight days in July 2011, as part of the NASA Earth Venture-1 DISCOVER-AQ (Deriving Information on Surface Conditions from Column and Vertically Resolved Observations Relevant to Air Quality, <http://www-air.larc.nasa.gov/missions/discover-aq/discover-aq.html>) field program. Measurements usually began between 7:00 and 10:00 local time and continued for about 8 h. Flights occurred over a range of weather conditions including clean days, pollution episodes, and weekdays and weekends. The P-3B aircraft housed two well-characterized in situ NO<sub>2</sub> measuring instruments: The University of California, Berkeley thermal dissociation laser induced fluorescence (TD-LIF, (Thornton et al., 2000; Wagner et al., 2011) and the National Center for Atmospheric Research (NCAR) 4-channel chemiluminescence instrument (P-CL). The P-CL measures NO<sub>2</sub> by photolysis of NO<sub>2</sub> and chemiluminescence detection of the product NO (Ridley and Grahek, 1990; Ridley et al., 2004). The TD-LIF instrument had a low NO<sub>2</sub> sampling frequency due to an alternating measurement cycle for other species such as peroxy nitrates, alkyl nitrates, and nitric acid, so we use measurements from the NCAR P-CL. The instrument has an NO<sub>2</sub> measurement uncertainty of 10% and a 1 s, 2 $\sigma$  detection limit of 50 ppt, making it useful to measure NO<sub>2</sub> in the free troposphere.

150 Figure 1 shows a typical in situ NO<sub>2</sub> measurement pattern during DISCOVER-AQ. Flight tracks for this campaign targeted urban air pollution spatially along the Interstate 95 (I-95) corridor in the Baltimore-Washington, D.C. region and vertically over the Chesapeake Bay and six surface air quality monitoring sites (see Table 1). Typically, during each sortie, three vertical spirals were flown over each location, covering altitudes from  $\sim 300$  m, in the boundary layer to  $\sim 3.3$  km, in the free troposphere. Table 1 provides the details on the number of spirals and observations and the measured altitude range. There were a total of 13–19 P-3B spirals over each surface site with 5356–15 827 1 s

observations made near the time of the OMI overpass. We found that the limited vertical extent of the aircraft pass over I-95 and the Chesapeake rendered those measurements less useful. We binned the measurements to the pressure grid of the GMI model to directly compare the model profiles with  
160 observed profiles, and to estimate the retrieval error due to the difference.

Figures 1 and 2 show the early afternoon (12:00–15:00) NO<sub>2</sub> vertical profiles measured during DISCOVER-AQ. NO<sub>2</sub> mixing ratios over land range over 0.02–28 ppb below 950 hPa, decrease sharply to 0.01–2 ppb at ~ 800 hPa, and are 10–200 ppt above 700 hPa. Over the Chesapeake Bay, NO<sub>2</sub> mixing ratios are generally less than 1 ppb, and the vertical gradient in the profile is less pronounced due to limited surface sources and transported NO<sub>2</sub> downwind. Large spatial and temporal  
165 variability in near-surface NO<sub>2</sub> reflect the large spatiotemporal variation in NO<sub>x</sub> emissions and differences in local dynamics. NO<sub>2</sub> enhancement and variability over Beltsville and Essex are largely due to local emissions, mostly from traffic. Most sites experienced more than factor-of-two greater NO<sub>2</sub> concentrations on highly polluted days with a shallow mixed layer on 5, 10, 21, and 28 July.

The aircraft measurements show that NO<sub>2</sub> concentrations within the mixed layer make the largest contributions to tropospheric NO<sub>2</sub> columns. The lowest 1 km of sampled aircraft data contain 64–84 % of the NO<sub>2</sub> column below 5 km. The same altitude range in the GMI profile represents 72–83 %, providing confidence in the GMI simulation. In the free troposphere (2–5 km), NO<sub>2</sub> concentrations from the a priori GMI climatology and aircraft measurements generally agree to within  
175 0.03 ppb. GMI simulations suggest that the NO<sub>2</sub> partial column within first few hundred meters from the ground to the lowest aircraft altitude comprise 30–40 % of the total column. The upper tropospheric column above 5 km is rather small, consisting of 10–15 % of the total column. We inferred the complete P-3B tropospheric NO<sub>2</sub> column by combining the measured values with GMI climatology above the highest aircraft level and extrapolating below the lowest aircraft level. The  
180 extrapolation scheme applies the vertical gradient of the NO<sub>2</sub> concentrations between the lowest aircraft altitude ( $C_M^j$ ) and underneath ( $C_M^{j-1}$ ) in the GMI profiles to the measured concentration ( $C^j$ ) to estimate concentration ( $C^{j-1}$ ):

$$C^{j-1} = \frac{C_M^{j-1}}{C_M^j} \times C^j, \quad (1)$$

185 where the subscript “M” represents model. In this approach, we assume that the GMI model captures the vertical distribution of NO<sub>2</sub> well.

We first evaluated the extrapolation scheme by comparing the estimated surface NO<sub>2</sub> mixing ratios with NO<sub>2</sub> measurements from a photolytic converter instrument at Padonia. Since NO<sub>2</sub> measurements at the lowest aircraft altitude are on average 45 % lower than the measurements at the  
190 ground, extrapolation of aircraft profiles by assuming a constant mixing ratio from the value at the lowest aircraft level will substantially underestimate the true NO<sub>2</sub> near the surface. In Figure 3, we show a comparison of our estimates using Eqn. 1 with surface measurements at Padonia. The extrapolated and measured values are well correlated ( $r = 0.64$ ,  $N = 14$ ), and generally compare well

(mean bias = 23 %), although extrapolation could at times overestimate observations when the aircraft encountered elevated plumes with high NO<sub>2</sub> concentrations. Errors in the calculated gradient propagate into the extrapolated value, degrading the quality of integrated P-3B tropospheric NO<sub>2</sub> columns. Allowing factor-of-two extrapolation errors, the errors in the integrated P-3B tropospheric NO<sub>2</sub> columns are generally less than 20 %.

### 2.3 Ground-based MAX-DOAS

Tropospheric NO<sub>2</sub> columns were measured by the ground-based MAX-DOAS instruments for several months during 2006–2011 at a remote site in Hedo and a suburban site in Tsukuba, Japan. NO<sub>2</sub> observations at these sites allow us to assess the OMI retrievals for contrasting environments (rural vs. urban).

The MAX-DOAS instrument measures scattered sunlight observations in the UV/visible wavelengths at several elevation angles between the horizon and zenith (e.g. Hönninger et al., 2004; Irie et al., 2012). Spectral fitting of the MAX-DOAS measured differential structure with absorption cross-section of NO<sub>2</sub> from Vandaele et al. (1998) at 294 K and other interfering species including O<sub>2</sub>–O<sub>2</sub>, O<sub>3</sub>, H<sub>2</sub>O, and the Ring and undersampling effects over the 460–490 nm window yields the differential slant column density, i.e., the difference in integrated columns along the average light path between measurements made at low elevation angles and that at an elevation angle of 90°. The accuracy of the retrieved NO<sub>2</sub> slant columns is ~ 10 %, as confirmed by a formal semi-blind inter-comparison experiment involving MAX-DOAS observations from different research groups (Roscoe et al., 2010). The NO<sub>2</sub> slant column densities are converted to tropospheric vertical column density by using the AMF calculated with measured aerosol information and the vertical profile of NO<sub>2</sub> and a non-linear iterative inversion scheme (Irie et al., 2012). Additional details on the MAX-DOAS measurements, calibration, and retrieval procedures can be found in Irie et al. (2008) and references therein. Overall errors in the tropospheric NO<sub>2</sub> vertical columns are < 14 %.

The MAX-DOAS instrument observes air masses representative of horizontal distance of about 10 km (Irie et al., 2012), comparable to the OMI spatial resolution. The temporal resolution corresponds to a complete sequence of elevation angles lasting for 30 min. We use the MAX-DOAS measurements taken within 30 min of OMI overpasses to compare with the OMI retrievals.

### 2.4 Ground-based Pandora

The direct sun total NO<sub>2</sub> column measurements were carried out at 12 DISCOVER-AQ sites (including six aircraft spiral locations) in Maryland and at the Chemistry and Physics Atmospheric Boundary Layer Experiment (CAPABLE) site at NASA’s Langley Research Center in Hampton, Virginia. The CAPABLE site is located in a coastal suburban area, which could experience sporadic local and transported NO<sub>x</sub> emissions. Additional details on the CAPABLE site can be found in Knepp et al. (2013). These measurements are useful to examine spatial and temporal variation in the

OMI retrievals.

230 Pandora is a ground-based spectrometer that measures direct solar irradiance over the range 280–  
525 nm at the spectral resolution of 0.6 nm, allowing the retrieval of the total column abundance of  
various species, such as O<sub>3</sub>, NO<sub>2</sub>, HCHO, H<sub>2</sub>O, and SO<sub>2</sub> (Herman et al., 2009). An algorithm for  
the retrieval of NO<sub>2</sub> from Pandora is similar to the direct-sun NO<sub>2</sub> inversion method from a Brewer  
spectrometer (Cede et al., 2006). The direct-sun DOAS technique is equally sensitive to stratospheric  
235 and tropospheric NO<sub>2</sub>, and is not affected by the Ring effect. The algorithm initially retrieves  
the relative NO<sub>2</sub> slant columns by least-square fitting of the difference between the logarithm of  
a reference irradiance spectrum and the logarithm of measured irradiance spectra with the absorption  
spectra of NO<sub>2</sub> (Vandaele et al., 1998) at 254.5 K and other atmospheric absorbers, a low-order  
polynomial, and wavelength shift and squeeze functions in the spectral range 370–500 nm. The  
240 temperature dependence of the NO<sub>2</sub> cross section is not accounted for in the fitting process. The  
differential NO<sub>2</sub> slant columns represent the difference between the absolute slant columns in the  
measured and the reference spectrum used for normalization. The reference spectrum is an average  
spectrum measured on clear clean days. The absolute slant column in the reference spectrum is  
determined by the Minimum-Amount Langley-Extrapolation method, as described in Herman et al.  
245 (2009). The direct sun AMF can be approximated as the secant of solar zenith angle and therefore  
does not require radiative transfer calculations or prior knowledge of the ground reflectivity or NO<sub>2</sub>  
profile shape.

The Pandora spectrometer provides NO<sub>2</sub> vertical column observations with a clear-sky precision  
of about  $2.7 \times 10^{14}$  molec. cm<sup>-2</sup> and a absolute accuracy of  $2.7 \times 10^{15}$  molec. cm<sup>-2</sup>. NO<sub>2</sub> column  
250 retrievals from Pandora have been previously validated against direct-sun Multi-Function DOAS  
(MFDOAS) and Fourier Transform Ultraviolet Spectrometer (UVFTS) data and have been found to  
agree to within 12 % (Piters et al., 2012; Wang et al., 2010; Herman et al., 2009). Here, we compute  
30 min Pandora column averages close to the OMI overpass time to compare with the nearest OMI  
NO<sub>2</sub> columns representing individual field of view (FOV). The maximum allowed collocation radius  
255 (distance between the center of the OMI FOV and the Pandora site) is 10 km.

## 2.5 In situ surface measurements

In situ measurements of surface NO<sub>2</sub> were made at the South Eastern Aerosol Research and CHaracterization (SEARCH) network, consisting of 7 sites in the Southeastern United States (Edgerton et al., 2006). We use data from two regionally representative sites: Centreville, in Alabama, and  
260 Yorkville, in Georgia measured during 2006–2009. Other sites that are either urban/suburban or  
located in close proximity to urban facilities were not found to be suitable for validation of satellite retrievals. NO<sub>2</sub> measurements are made using photolytic converter analyzers, a measurement method that employs photolysis of ambient NO<sub>2</sub> followed by chemiluminescence detection of the product NO. This method offers highly accurate NO<sub>2</sub> measurements, with an uncertainty < 10 %.



**3.1 NO<sub>2</sub> profile shapes**

We initially evaluate the a priori monthly mean relative vertical distribution (shape factor) of NO<sub>2</sub> used in the OMI NO<sub>2</sub> retrievals with aircraft measurements during the DISCOVER-AQ field campaign. Figure 4 compares average NO<sub>2</sub> shape factors over various locations from aircraft with those  
270 calculated with the GMI model. Although the aircraft measurements are qualitatively similar to the model results, differences up to 30% were observed near the surface and in the free-troposphere. The GMI model suggests that 20–30% of the tropospheric NO<sub>2</sub> column is located near the surface (first model layer, ~ 1000 hPa), while only 5–10% is in the mixed layers between 900–1000 hPa, and less than 3% is in the free-troposphere (< 900 hPa). Aircraft measurements indicate the hori-  
275 zontal spatial gradient in the free-tropospheric shape factors, primarily due to the dominant lower tropospheric contributions to the total tropospheric NO<sub>2</sub> columns in urban source regions. These measurements also reveal considerable day-to-day variation in NO<sub>2</sub> profile shapes within a given month, suggesting that the use of a monthly mean profile in the operational algorithm is potentially a significant source of error in individual retrieved tropospheric NO<sub>2</sub> columns.

**280 3.2 Tropospheric NO<sub>2</sub> columns****3.2.1 Comparison with in situ aircraft measurements**

In this section, we compare OMI tropospheric NO<sub>2</sub> columns with integrated columns from aircraft spirals at six locations in Maryland during the DISCOVER-AQ field campaign in July 2011. We select only the spirals made within 1 h of the OMI overpass. Not all data from the 14 flight days  
285 could be used due to adverse instrumental (row anomaly) or cloudy conditions affecting the OMI data.

Figure 5 shows tropospheric NO<sub>2</sub> columns from OMI and vertically integrated in situ aircraft measurements for several individual flight days. Individual measurements agree to within 20% in 60% of cases at Fair Hill, Aldino, Padonia, and Beltsville. A more substantial difference was  
290 observed at Edgewood and Essex, where aircraft measurements were systematically higher than OMI retrievals. These two coastal towns were often impacted by a bay breeze, yielding complex vertical and horizontal distributions of NO<sub>2</sub>. Figure 6 shows a summary of comparisons at all DISCOVER-AQ sites. Although OMI and the in situ tropospheric NO<sub>2</sub> columns are highly correlated at some sites, the overall correlation at all sites is rather poor ( $r = 0.2$ ,  $N = 59$ ). The observed discrepancy  
295 between the two measurements is primarily due to the difference in spatial sampling, but it could also be due to other reasons, such as errors in OMI tropospheric NO<sub>2</sub> due to inaccurate removal of stratospheric NO<sub>2</sub> on 2 July and partly cloudy conditions obstructing the scene on 20 July.

Figure 7 shows the campaign average tropospheric NO<sub>2</sub> columns observed by the OMI and air-

craft instruments. Measurements from both instruments exhibit a distinct spatial variation, with low  
300 columns at the rural site Fair Hill and high columns in urban sites such as Beltsville and Essex.  
NO<sub>2</sub> retrievals from OMI are lower than aircraft measurements by 5.8–22.1 %, with the exception  
of Edgewood and Essex, where aircraft measurements are often up to a factor of two higher than  
OMI retrievals. We quantify the impact of the a priori NO<sub>2</sub> profiles in the OMI retrievals for the  
observed discrepancy between OMI and in situ measurements in Sect. 4.

### 305 3.2.2 Comparison With Pandora Measurements

We compare OMI total NO<sub>2</sub> columns (sum of tropospheric and stratospheric columns) with Pandora  
direct sun NO<sub>2</sub> column retrievals at six sites in Maryland during the first DISCOVER-AQ field cam-  
paign in July 2011 and at the CAPABLE site at NASA Langley in Hampton, Virginia for 2010–2012.  
Although analysis of Pandora measurements allows inference of the stratospheric portion of the to-  
310 tal NO<sub>2</sub> column (Herman et al., 2009), the separate stratospheric and tropospheric components are  
not currently available from Pandora. Subtraction of OMI-derived stratospheric NO<sub>2</sub> columns from  
Pandora total column measurements could as well introduce errors in Pandora-derived tropospheric  
NO<sub>2</sub> columns. Therefore the use of total columns allows us to reduce these errors, and allows more  
direct comparison between the two measurements.

315 Figures 6 and 8 present a comparison of coincident total NO<sub>2</sub> column retrievals from the OMI and  
Pandora instruments. The variations of OMI NO<sub>2</sub> are broadly consistent with the Pandora measure-  
ments. Although the OMI and Pandora NO<sub>2</sub> columns are fairly correlated ( $r = 0.25$ ,  $N = 52$ ), they  
generally agree to within 18 % at Aldino and Beltsville and within 30 % at the other DISCOVER-  
AQ sites. Occasional large discrepancies are evident, reflecting a combination of enhanced spatial  
320 variation and placement of the Pandora spectrometers.

Figure 7 shows campaign average total NO<sub>2</sub> columns measured by Pandora and OMI at six  
DISCOVER-AQ sites in Maryland. The measurements are in good agreement. NO<sub>2</sub> columns mea-  
sured with the Pandora are on average < 6 % higher at Aldino, Beltsville, and Edgewood, and 9–  
13 % lower than OMI at Padonia and Essex. Inconsistent results at Fair Hill, with a high bias in  
325 the OMI retrievals (44 %) vs. Pandora and a low bias (6.7 %) vs. aircraft measurements, suggest  
differences in sampling area by the three independent measurement systems.

We also compare long-term observations of the total NO<sub>2</sub> columns by the OMI and Pandora  
instruments at the CAPABLE site. Figure 9 shows the multi-year monthly mean variation of OMI  
and Pandora NO<sub>2</sub> columns. NO<sub>2</sub> retrievals from the two instruments are moderately correlated ( $r =$   
330  $0.5$ ,  $N = 163$ ), with the largest correlation ( $r = 0.71$ ,  $N = 40$ ) in winter and smallest correlation  
( $r = 0.25$ ,  $N = 33$ ) in spring. However, the magnitude of the seasonal cycle differs for the two  
measurements, and they are not in phase. The seasonal variation in Pandora NO<sub>2</sub> columns exhibits  
a summer maximum and fall minimum, in contrast to the winter maximum and summer minimum  
in OMI total columns. The monthly mean biases range from –2.8 % in January to –28.4 % in June

335 (Pandora being higher). The seasonal cycle in tropospheric and stratospheric NO<sub>2</sub> columns retrieved  
from OMI and simulated from GMI are highly consistent (not shown), providing confidence in the  
seasonal variation in the OMI retrievals. Several factors could contribute to the observed seasonal  
biases between the OMI and Pandora retrievals. Due to the close proximity to local traffic at Langley  
Air Force Base, and the Yorktown power plant, Pandora measurements are influenced by local NO<sub>x</sub>  
340 emission sources and could exhibit a dampened seasonal tropospheric NO<sub>2</sub> cycle. Also, unlike the  
OMI retrievals, the Pandora retrievals are based on the NO<sub>2</sub> cross-section at a constant temperature  
of 255 K (representing the stratosphere and troposphere), which could affect seasonal variation in  
the retrieved NO<sub>2</sub> columns. However, the effect of the temperature error in Pandora data is small  
(~ 3.3 % per 10° change in NO<sub>2</sub> temperature) and is unlikely to explain the observed seasonal  
345 differences. Errors in absolute calibration could lead to  $\pm 2.7 \times 10^{15}$  molec. cm<sup>-2</sup> uncertainty in  
Pandora NO<sub>2</sub> slant columns, with a similar uncertainty in vertical columns in summer, but only half  
of that in winter, favoring wintertime data, which are in excellent agreement with the OMI retrievals.

### 3.2.3 Comparison with MAX-DOAS measurements

Tropospheric NO<sub>2</sub> column retrievals from OMI are compared with long-term MAX-DOAS mea-  
350 surements at two Japanese sites, Tsukuba and Hedo, for the period 2006–2011. Figure 10 (left)  
compares tropospheric NO<sub>2</sub> columns retrieved from OMI and MAX-DOAS instruments. Tro-  
pospheric NO<sub>2</sub> columns over Hedo range over  $0.2\text{--}3.2 \times 10^{15}$  molec. cm<sup>-2</sup> for MAX-DOAS and  
 $-0.5\text{--}2.8 \times 10^{15}$  molec. cm<sup>-2</sup> for OMI. The stratosphere–troposphere separation scheme in the OMI  
retrievals could yield slightly negative tropospheric columns in remote areas when measured slant  
355 columns are lower than estimated stratospheric slant columns. NO<sub>2</sub> columns over Tsukuba are much  
higher, reaching  $40 \times 10^{15}$  molec. cm<sup>-2</sup> in both the MAX-DOAS and OMI data. Measurements from  
the two techniques exhibit a significant spatio-temporal correlation ( $r = 0.86$ ,  $N = 626$ ). The mean  
relative difference between OMI and MAX-DOAS measurements is  $-16.3\%$  in Tsukuba and  $7.1\%$   
in Hedo.

360 Figure 10 (right) presents the seasonal mean tropospheric NO<sub>2</sub> column from MAX-DOAS mea-  
surements and those retrieved from OMI. The seasonal variation of the OMI-retrieved NO<sub>2</sub> columns  
is consistent with the MAX-DOAS measurements. The seasonal mean NO<sub>2</sub> columns for the MAX-  
DOAS measurements decrease by a factor of 1.6–1.9 from winter to summer, compared with a factor  
of 1.4–1.5 for OMI. The relative difference between OMI and MAX-DOAS seasonal mean tropo-  
365 spheric NO<sub>2</sub> columns range from 0.5 % in fall to  $-20.8\%$  in winter at Tsukuba and from  $-21.3\%$   
in winter to 24.8 % in spring at Hedo. These results are generally consistent with the comparisons  
made with aircraft and Pandora observations.

### 3.2.4 Comparison with in situ surface measurements

We conduct an indirect validation of cloud-free (cloud radiance fraction  $< 0.5$ ) OMI tropospheric  
370  $\text{NO}_2$  columns by comparison with coincident hourly in situ surface  $\text{NO}_2$  measurements. This ap-  
proach requires estimating ground-level  $\text{NO}_2$  concentrations from OMI. We follow the method of  
Lamsal et al. (2008) with improvements as described in Lamsal et al. (2013) that combines coinci-  
dently sampled  $\text{NO}_2$  vertical profile taken from a GEOS-Chem nested simulation (see Appendix B)  
with the OMI observations containing information about the spatial variation of the tropospheric  
375  $\text{NO}_2$  columns in the boundary layer. The OMI-derived surface  $\text{NO}_2$  represents the mean mixing  
ratio in the lowest vertical layer ( $\sim 50$  m) of the model.

We compare the OMI-derived surface  $\text{NO}_2$  mixing ratios with the in situ measurements at the  
two rural surface sites, in Yorkville and Centerville for 2006–2010. Figure 11 displays the seasonal  
average surface  $\text{NO}_2$  mixing ratios from the in situ measurements and those derived from the OMI  
380 retrievals. The OMI-derived surface  $\text{NO}_2$  concentrations are well correlated with the photolytic  
converter measurements ( $r = 0.61$ ,  $N = 700$  for Yorkville and  $r = 0.69$ ,  $N = 676$  for Centerville)  
and exhibit similar seasonal variation with summertime minima. The OMI-derived surface  $\text{NO}_2$  are  
lower than the in situ measurements at Centerville by 11.8 % in fall but higher by 4.1 % in spring.  
Discrepancies are larger at Yorkville, where the OMI-derived surface  $\text{NO}_2$  overestimates in situ  
385 measurements by 8.2 % in spring and underestimates by 25–31 % in other seasons.

### 3.2.5 Comparison with bottom-up emissions

We use an inventory of US  $\text{NO}_x$  emissions to indirectly validate OMI tropospheric  $\text{NO}_2$  columns.  
We employ the emissions for 2005 as implemented in the GEOS-Chem model (Appendix B). Emis-  
sions employed by the GMI (Appendix A) simulation used in the operational retrieval included  
390 outdated North American  $\text{NO}_x$  emissions not suitable for validation. In GEOS-Chem, the bottom-  
up emissions over the US comprise over 75 % of  $\text{NO}_x$  emissions from anthropogenic activities; the  
remainder comes from soil, lightning, and biomass burning emissions. In contrast to inventories  
in developing countries, the US national emission inventory is more complete, accurate, and trans-  
parent (NARSTO, 2005), and is expected to be less uncertain ( $< 25$  %, Christian Hogrefe, personal  
395 communication, 2008) at least in national totals. The largest contributors to the US  $\text{NO}_x$  emissions  
include on- and off-road vehicles ( $\sim 62$  %) and electricity and industrial power generation ( $\sim 27$  %),  
which exhibit little seasonal variation (EPA, 2009; Lamsal et al., 2010), a characteristic that is use-  
ful to assess seasonal variation in OMI retrievals. Difficulty could arise for comparisons focussed  
on county or sectoral levels, where uncertainty in bottom-up emissions could be significant, and in  
400 spring and summer, when emissions from soils and biomass burning are at peak levels.

To compare the OMI retrievals with  $\text{NO}_x$  emissions, we follow a simple mass balance approach  
(Martin et al., 2003; Lamsal et al., 2010), which directly relates OMI tropospheric  $\text{NO}_2$  columns ( $\Omega$ )

to surface NO<sub>x</sub> emissions ( $E$ ):

$$E = \frac{E_M}{\Omega_M} \times \Omega. \quad (2)$$

Here,  $\Omega_M$  is the tropospheric NO<sub>2</sub> column from a GEOS-Chem nested simulation based on the a priori surface NO<sub>x</sub> emissions  $E_M$ , both sampled at the OMI overpass time. To account for the impact of spatial smearing (Palmer et al., 2003), we considered an approach that accounts for the emissions from eight adjacent model grid cells to estimate surface NO<sub>x</sub> emissions ( $E_{i,j}$ ) at grid cell ( $i, j$ ) from OMI (Toenges-Schüller et al., 2006; Boersma et al., 2008a; Lamsal et al., 2010) with improvements as discussed in Tang et al. (2013):

$$E_{i,j} = \frac{E'_{M_{i,j}}}{\sum_{n=-1}^1 \sum_{m=-1}^1 K_{i,j} E'_{M_{i+m,j+n}}} \times \frac{E_{M_{i,j}}}{\Omega_{M_{i,j}}} \times \Omega_{i,j}. \quad (3)$$

The smoothing kernel ( $K$ ) is defined as  $\frac{1}{p+8} \begin{bmatrix} 1 & 1 & 1 \\ 1 & p & 1 \\ 1 & 1 & 1 \end{bmatrix}$ , where  $p$  is the smoothing parameter. To

determine the value of  $p$ , we applied  $K$  to each grid cell in the bottom-up NO<sub>x</sub> emission inventory with different  $p$  values, and computed the correlation between smoothed 24 h averaged bottom-up NO<sub>x</sub> emissions ( $E'_{i,j}$ ) and corresponding modeled tropospheric NO<sub>2</sub> columns. The maximum correlation coefficient corresponding to the optimal value of  $p$  was achieved at  $p = 12$  as in Boersma et al. (2008a), which we adopt to infer monthly top-down surface NO<sub>x</sub> emissions from OMI.

Figure 12 shows the spatial variation of bottom-up and OMI-based top-down NO<sub>x</sub> inventories of land surface emissions. Both top-down and bottom-up inventories exhibit similarity in their spatial patterns, with large emissions in major urban centers, reflecting industrialization, dense traffic and population. The top-down and bottom-up annual surface NO<sub>x</sub> emissions are strongly correlated ( $r = 0.95$ ,  $N = 2706$ ). The difference between the OMI-derived and bottom-up annual surface NO<sub>x</sub> emissions integrated over the continental US is 8.8 %, much lower than the uncertainty in the bottom-up inventory and in the daily OMI retrievals. Excluding the smoothing parameter in the inversion, the difference decreases to 3.5 %. Despite excellent agreement in the total surface NO<sub>x</sub> emissions, we observe a pronounced difference of up to a factor-of-two in the magnitude of local and regional NO<sub>x</sub> emissions. These differences could arise from errors in the bottom-up emissions, in the OMI retrievals, and from the simple inversion scheme.

Figure 12 (bottom right) shows the ratio of the seasonal area-integrated OMI-derived and bottom-up NO<sub>x</sub> emissions over the US. The ratio ranges from 0.91 in July to 1.35 in April. These results suggest consistency between bottom-up emissions and OMI retrievals within the range of their uncertainties.

### 435 3.2.6 Synthesis of validation results

Direct validation results of OMI NO<sub>2</sub> retrievals vs. in situ aircraft, MAX-DOAS, and ground direct sun Pandora measurements, and indirect validation results of OMI-derived surface NO<sub>2</sub> vs. in situ surface measurements and top-down vs. bottom-up emission inventories suggest the scientifically useful quality of the archived tropospheric NO<sub>2</sub> product from the standard OMI operational algorithm. Table 2 contains a summary of these validation results. OMI tropospheric NO<sub>2</sub> data generally correlate well ( $r > 0.5$ ), agree to within  $\pm 20\%$  with biases tending to be more negative than positive, and exhibit similarity in monthly/seasonal variation with the independent data sets. These results are impressive considering the inherent limitations associated with the uncertainties in OMI retrievals and currently available validation data sets. Both temporal and spatial incoherence causes complications in comparing satellite observations with ground-based and aircraft measurements and can often result in misleading conclusions. NO<sub>2</sub> in the lower troposphere is short-lived and is concentrated close to emission sources. Ground-based and in situ instruments offer local measurements, in contrast to satellite observations averaged over a large field of view covering several hundred square kilometres. Therefore, differences between the two measurements ought to be expected simply due to NO<sub>2</sub> spatial inhomogeneity. The sampling differences can be reduced by acquiring long time series of NO<sub>2</sub> measurements, preferably in background locations with more homogeneous distributions.

Although OMI tropospheric NO<sub>2</sub> retrievals show promise and generally compare well with ground truth, occasional large differences could be due to errors in OMI tropospheric NO<sub>2</sub> columns. Principal sources of error in OMI tropospheric column density are radiometric errors, slant column density calculation, the air mass factor, the retrieved cloud parameters, and the stratosphere–troposphere separation procedure. The tropospheric air mass factor is highly sensitive to errors in surface reflectivity in polluted areas with low surface reflectivity (e.g. Boersma et al., 2004). Further, the tropospheric air mass factor is calculated assuming the NO<sub>2</sub> retrieval implicitly accounts for aerosols through OMI-retrieved cloud fraction and surface reflectivity. However, algorithmic bias due to the presence of actual aerosols has not been studied. We quantify the impact of the a priori NO<sub>2</sub> profiles in tropospheric NO<sub>2</sub> retrievals in Sect. 4.

#### 4 Effect of NO<sub>2</sub> profiles in NO<sub>2</sub> retrievals

In this section, we use aircraft in situ NO<sub>2</sub> measurements coincident with OMI observations during the DISCOVER-AQ campaign in Maryland to explore the sensitivity of the retrieved tropospheric columns to the a priori profiles.

Conversion of the slant column ( $\Omega_s$ ) retrieved from the satellite-measured reflectance spectrum  $y$

to vertical NO<sub>2</sub> column ( $\Omega_v$ ) requires an AMF ( $A$ ):

$$\Omega_v = \frac{\Omega_s(y)}{A(x_a, b)}. \quad (4)$$

The AMF, a measure of the sensitivity of  $\ln(y)$  to NO<sub>2</sub>, depends on both the a priori NO<sub>2</sub> profile  $x_a$  and the forward model parameters  $b$ , which include the optical geometry and atmospheric and surface properties (surface albedo, cloud fraction, and cloud height). NO<sub>2</sub> is optically thin in the visible; this allows the calculation of AMF with a profile of altitude-dependent scattering weights

( $w$ ) computed from a radiative transfer model and the a priori NO<sub>2</sub> profile shape:

$$A_{\text{trop}} = \frac{\sum_{\text{surface}}^{\text{tropopause}} w \times x_a}{\sum_{\text{surface}}^{\text{tropopause}} x_a}, \quad (5)$$

where  $x_a$  is the partial NO<sub>2</sub> column. The scattering weights include layer-specific correction factors to account for the temperature dependence of the NO<sub>2</sub> absorption cross-section. The summation extending from the surface to the tropopause provides tropospheric AMF ( $A_{\text{trop}}$ ).

We use Eq. (5) to re-compute tropospheric AMF ( $A_{\text{trop.ac}}$ ) using the measured NO<sub>2</sub> vertical profiles from aircraft and re-calculate tropospheric NO<sub>2</sub> column  $\Omega_{v, \text{trop.ac}}$  from OMI tropospheric slant columns ( $\Omega_{s, \text{trop}}$ ):

$$\Omega_{v, \text{trop.ac}} = \frac{\Omega_{s, \text{trop}}}{A_{\text{trop.ac}}} = \frac{\Omega_s - \Omega_{s, \text{strat}}}{A_{\text{trop.ac}}}. \quad (6)$$

Here,  $\Omega_s$  is the de-striped NO<sub>2</sub> slant column density (measured NO<sub>2</sub> slant column corrected for instrumental artifacts). The stratospheric slant columns ( $\Omega_{s, \text{strat}}$ ) are calculated from the stratospheric NO<sub>2</sub> vertical columns and the stratospheric AMF, both available in the operational data product.

Figures 5–8 contain tropospheric NO<sub>2</sub> columns re-calculated with aircraft-measured NO<sub>2</sub> vertical profiles. The OMI NO<sub>2</sub> retrievals calculated using the aircraft measured profiles differ from the operational retrievals calculated with model-simulated profiles by up to –43 %, in line with other estimates using high resolution a priori profiles (Heckel et al., 2011; Russell et al., 2011). Compared to the operational retrievals, the new retrievals are systematically lower by 16–19 % in rural locations and higher by 15–21 % in urban locations. These results are consistent with the previous study by Hains et al. (2010), who evaluated the impact of a priori profiles in the Dutch NO<sub>2</sub> (DOMINO) retrievals using observations from the Dutch Aerosol and Nitrogen Dioxide Experiments for validation of OMI and SCIAMACHY (DANDELIONS) and Intercontinental Chemical Transport Experiment Phase B (INTEX-B) campaigns. Our use of measured profiles improved the correlation between OMI and aircraft measurements ( $r = 0.5$ ,  $N = 59$ ). Overall, the agreement between OMI and aircraft measurements improved in urban locations by 12–14 % and worsened at Aldino and Fair Hill by a similar magnitude. Comparison of the OMI NO<sub>2</sub> retrievals calculated using the aircraft measured profiles with Pandora observations are presented in Figures 6–8. Except for Fair Hill, the correlation of OMI with Pandora improved with the new retrievals ( $r = 0.4$ ,  $N = 52$ ). The bias of the OMI retrievals against Pandora reduced at Fair Hill, Beltsville, and Edgewood, but increased at Aldino, Padonia, and Essex.

## 5 Use of scattering weights in applications of OMI to evaluate AQ models

Several studies (e.g. van Noije et al., 2006; Lamsal et al., 2010) have compared model-simulated NO<sub>2</sub> columns with satellite retrievals. Such comparisons require coincident sampling of model output with observations, because inconsistent sampling could lead to significant differences and  
510 incorrect interpretation of the data. The most common approach to comparison involves examining and interpreting the difference between satellite observations and model results. This approach of direct comparison is expected to have difficulty when interpreting differences unless the a priori NO<sub>2</sub> vertical profile shapes used in the retrievals are from the model in question. In this section, we offer an example of the use of scattering weights and OMI retrievals to evaluate AQ models.

515 The operational NO<sub>2</sub> retrieval algorithm uses NO<sub>2</sub> shape factors generated from GMI simulation results, available at the resolution of 2° × 2.5°. The coarse-resolution model profiles may not sufficiently capture the actual vertical distribution of NO<sub>2</sub>, especially where the horizontal gradient is large. Moreover, over the last decade, anthropogenic emissions of NO<sub>x</sub> have undergone rapid changes that may change the local NO<sub>2</sub> shape factor and subsequently affect the retrieval of tropo-  
520 spheric NO<sub>2</sub>. Use of profiles obtained from a model simulation performed with updated emissions at high resolution not only lead to more accurate retrievals through improved spatial representation of NO<sub>2</sub> shape factors in the AMF calculation, but it also ensures self-consistency when the OMI retrievals are compared with modeled NO<sub>2</sub> columns (Eskes and Boersma, 2003; Boersma et al., 2004).

525 Here, we show an example by comparing OMI tropospheric NO<sub>2</sub> retrievals with a model simulation. We consider the GEOS-Chem nested model (Appendix B) for North America that includes updated emissions and performs simulation at high resolution 0.5° × 0.667°. As compared to the coarse model simulation, the fine model simulation can provide better representation of the vertical distributions of NO<sub>2</sub> in OMI pixels by considering changes in the NO<sub>2</sub> shape factors related to the  
530 changes in NO<sub>x</sub> emissions. We use Eq. (5) to re-compute the tropospheric AMF ( $A_{\text{trop\_GC}}$ ) using the new profile and use Eq. (6) to re-calculate the tropospheric NO<sub>2</sub> column (OMI\_GC) from OMI. For comparison, we use OMI pixels with cloud radiance fraction < 0.5 and surface reflectivity < 0.3 and calculate area-weighted average columns (Level 3) on a 0.5° × 0.667° grid.

Figure 13 shows seasonal mean tropospheric NO<sub>2</sub> columns from OMI and GEOS-Chem for 2005.  
535 Both show large NO<sub>2</sub> columns in dense urban areas in eastern North America and major metropolitan areas such as Los Angeles, San Francisco, Denver, and Houston. They exhibit a similar seasonal pattern, with a winter maximum, reflecting longer NO<sub>x</sub> lifetime and shallower mixing layer depth in winter. The correlation between the GEOS-Chem model and OMI seasonal NO<sub>2</sub> columns is remarkable ( $r = 0.85\text{--}0.92$ ). The seasonal average GEOS-Chem column is lower than the OMI column by  
540 7 % in spring and higher by 24 % in summer yet within the estimated uncertainty of OMI retrievals and GEOS-Chem simulation.

OMI tropospheric NO<sub>2</sub> columns exhibit a number of differences with the modeled NO<sub>2</sub> columns



(Fig. 13, fourth row). The modeled NO<sub>2</sub> columns are generally larger in some urban areas of the west coast and northeastern US and over Alberta. Simulation from GEOS-Chem also indicates about  
545 factor-of-two higher columns in summer in the Midwest US, a major region of soil NO<sub>x</sub> emissions. Retrieved columns are higher over the eastern US in spring, eastern Canada in winter, and cleaner background areas in all seasons. Some of these differences could point to certain emission sources that are not well represented in the model or remaining retrieval biases such as due to the treatment of snow (O'Byrne et al., 2010; McLinden et al., 2014). Other sources of model bias include the errors  
550 in simulating OH concentrations, N<sub>2</sub>O<sub>5</sub> hydrolysis rates, and vertical mixing that affect simulation of NO<sub>x</sub> chemistry (van Noije et al., 2006; Valin et al., 2011).

Possible errors in OMI retrievals causing the observed difference cannot be ruled out. Due to several error sources in the AMF calculation, systematic biases in the spatial variation of OMI retrievals are expected. The spatial resolution of surface reflectivity and a priori NO<sub>2</sub> shape factor are coarser  
555 than the ground resolution of OMI, yielding errors in AMF. A change in surface reflectivity from 0.01 to 0.1 could alter the AMF by up to 90 % (Leitão et al., 2010), which suggests the importance of accurate knowledge of surface properties (McLinden et al., 2014) and potential impact of residual cloud contamination in the climatology of surface reflectivity. Some previous retrieval studies have used high-resolution MODIS albedo data in an attempt to reduce uncertainty in the tropospheric  
560 AMF (Russell et al., 2011; Zhou et al., 2009). Lack of explicit treatment of aerosols in the AMF calculation could have a significant impact in the retrieval of tropospheric NO<sub>2</sub>, although the effect could be moderate (7 %) over highly polluted areas (Leitão et al., 2010). Errors in retrievals could be quite large in cases of elevated aerosols in downwind areas, if those elevated aerosols are not accounted for.

565 Figure 13 (fifth row) shows the seasonal mean difference resulting from the use of GMI profile shapes in the AMF calculation. Since the GMI model and GEOS-Chem both use GEOS-5 meteorological fields and have similar tropospheric chemical mechanisms, the difference between the two retrievals is primarily due to differences in emissions. The anthropogenic emissions in the GMI simulation are appropriate for 1999, which is considerably higher than 2005 emissions over nearly all  
570 of North America, with the notable exception of Alberta, where it is considerably lower. Resulting changes in local NO<sub>2</sub> profile shape impact tropospheric AMFs and, therefore, change individual retrievals by up to 40 % and seasonal averages by 1 % in winter and 12 % in fall.

## 6 Conclusions

We compared the OMI tropospheric NO<sub>2</sub> product (OMNO2, version 2.1) to ground-based measure-  
575 ments to assess the data quality, and to aircraft-based measurements, both to compare the retrieved column amounts and to assess the sensitivity of OMI NO<sub>2</sub> to the a priori profiles used in the retrieval. Model profiles were used to estimate tropospheric column amounts from in situ measurements of

NO<sub>2</sub> at ground-level. Finally, we investigated the potential improvement of the retrievals that could be realized using a higher-resolution model, with updated emissions inputs, as a source of a priori profiles. Table 2 summarizes the results of these investigations.

We examined NO<sub>2</sub> profiles measured in situ by the NCAR chemiluminescence instrument flown in the P-3B aircraft during the DISCOVER-AQ field campaign in the Baltimore-Washington, D.C. metropolitan region in July 2011. The P-3B aircraft provided NO<sub>2</sub> measurements from ~ 300 m in the boundary layer to ~ 3.3 km in the free-troposphere, allowing evaluation of tropospheric NO<sub>2</sub> from OMI and estimation of retrieval errors due to a priori NO<sub>2</sub> profiles from the Global Modeling Initiative model. The mean relative vertical distribution of NO<sub>2</sub> from aircraft and that calculated with the GMI model are in agreement to within 30 %, but observations also reveal a significant day-to-day variability in NO<sub>2</sub> profile shape. Using aircraft NO<sub>2</sub> profiles altered tropospheric AMFs by up to 43 % on some days and yielded improved daily NO<sub>2</sub> column retrievals. Coincident OMI and aircraft measurements agree to within 20 % for a majority of cases, with low biases in OMI retrievals by 5.8–22.1 % at rural and urban locations and by 50 % in the coastal towns of Essex and Edgewood. Comparison of total NO<sub>2</sub> column measurements from OMI and Pandora instruments at those locations presented inconsistent results, suggesting low biases in OMI retrievals of < 6 % at Aldino, Beltsville, and Edgewood, and high biases of 9–13 % at Padonia and Essex. Spatial inhomogeneity within a satellite ground pixel, stratosphere–troposphere separation in OMI data, and differences in the sampling domain among the three measurements make short-term comparisons difficult.

We used ground-based data for an extended period of time to examine the seasonal variation of tropospheric NO<sub>2</sub> retrievals. Comparison with the MAX-DOAS measurements at a remote location in Hedo and an urban site in Tsukuba in Japan during 2006–2011 suggests that OMI and MAX-DOAS data are highly consistent ( $r = 0.86$ ), with seasonal biases < 25 % and a mean bias of –16.3 % at Tsukuba and 7.1 % at Hedo in the OMI retrievals. The inconsistent seasonal variation in total NO<sub>2</sub> columns from OMI and Pandora at Hampton, VA, likely arises from the influence of local NO<sub>x</sub> emission sources in the Pandora measurements.

As an indirect validation, we derived the ground-level NO<sub>2</sub> from OMI using coincident GEOS-Chem NO<sub>2</sub> profiles and compared them with surface NO<sub>2</sub> measurements at two rural sites (Centerville, AL and Yorkville, GA) of the SEARCH network. The mean seasonal difference between the OMI-derived surface NO<sub>2</sub> and surface measurements ranges from –11.8 % (fall) to 4.1 % (spring) in Centerville and from –31 % (winter) to 8.2 % (spring) in Yorkville. Use of well-established seasonal bottom-up surface NO<sub>x</sub> emissions inventories over the United States suggested that the monthly mean differences in OMI-derived top-down surface NO<sub>x</sub> emissions range from –9 % in July to 35 % in April.

Overall, despite the typical complexities associated with the validation of satellite retrievals, OMI tropospheric NO<sub>2</sub> columns are consistent with and agree within the uncertainty of the validation

615 datasets. Therefore, the OMI data offer the means to evaluate the fidelity of CTM model results. The comparison of model-simulated NO<sub>2</sub> columns with satellite retrievals should utilize scattering weights (or averaging kernels) that are made available with the OMI data files, to correct for the effect of climatological monthly a priori NO<sub>2</sub> profiles used in the retrievals. OMI retrieval algorithms could benefit from high-resolution surface reflectivity information and a priori NO<sub>2</sub> profiles and from the  
620 explicit treatment of aerosols.

The spatial and temporal coverage of the comparisons we have examined in this paper are limited; they may not be representative of other locations and seasons. A coordinated effort in generating validation datasets by including remotely sensed and in situ observations at the ground, with balloon sondes, and from aircraft over a wide geographic region for a long time period will be valuable for  
625 assessing satellite retrievals.

## Appendix A

### GMI model description

Retrieval of tropospheric NO<sub>2</sub> columns from a satellite instrument requires an assumed vertical distribution of NO<sub>2</sub>. Because NO<sub>2</sub> in situ profile measurements are very few, and because the spatial  
630 variability in NO<sub>2</sub> profiles is quite large, this is best achieved from a global three-dimensional chemical transport model for atmospheric composition. We use the Global Modeling Initiative (GMI) model (Strahan et al., 2007), consisting of a chemical mechanism that combines the stratospheric mechanism described in Douglass et al. (2004) with a version of the tropospheric mechanism in GEOS-Chem (Bey et al., 2001) with modifications as described in Duncan et al. (2007). The model  
635 is driven by assimilated meteorological fields from the Goddard Earth Observing System (GEOS) at the NASA Global Modeling and Assimilation Office (GMAO, <http://gmao.gsfc.nasa.gov/>). The GEOS-5 meteorological data are provided every 3–6 h (3 h for surface fields and mixing depths) at 72 pressure levels in the vertical, extending from surface to 0.01 hPa.

The model includes the global anthropogenic emissions from the Global Emission Inventory Activity [GEIA, (Benkovitz et al., 1996) for the base year of 1985 and scaled to 1995, as described in  
640 Bey et al. (2001). The global inventory is replaced by the following regional inventories: the US EPA National Emissions Inventory (NEI) for 1999 over the United States, the Criteria Air Contaminants (CAC) inventory (<http://www.ec.gc.ca/inrp-npri>) for 2000 over Canada, the Big Bend Regional Aerosol and Visibility Observational Study (BRAVO) inventory for 1999 over Mexico (Kuhns et al.,  
645 2005), the European Monitoring and Evaluation Programme (EMEP) inventory for 2000 over Europe, and the inventory from Streets et al. (2006) for 2006 over East Asia. The GMI model also includes NO<sub>x</sub> emissions from soil, lightning, biomass burning, biofuel, and aircraft sources, as described in Duncan et al. (2007).

In this work, the model simulation was conducted at the resolution of  $2^\circ \times 2.5^\circ$  for three years  
650 (2005–2007). Model outputs were sampled at the local time of OMI overpass. Since monthly mean  
values capture the seasonal variation, we derived monthly mean values for  $\text{NO}_2$  and temperature  
profiles and tropopause pressures needed for the calculation of the AMF.

## Appendix B

### GEOS-Chem model description

655 We use the GEOS-Chem three-dimensional model of tropospheric chemistry (Bey et al., 2001),  
version 9-01-03 ([www.geos-chem.org](http://www.geos-chem.org)), to demonstrate the application of scattering weights to re-  
calculate the OMI tropospheric  $\text{NO}_2$  column and to examine the effect of  $\text{NO}_2$  profile shape in  
retrievals of tropospheric  $\text{NO}_2$  columns. We employ GEOS-Chem nested simulations (Zhang et al.,  
2011; Wang et al., 2012; van Donkelaar et al., 2012; Lamsal et al., 2013) with a horizontal grid  
660 size of  $\frac{1}{2}^\circ \times \frac{2}{3}^\circ$  over North America ( $10\text{--}70^\circ \text{N}$ ,  $40\text{--}140^\circ \text{W}$ ). Boundary conditions of the nested  
region are provided by the global simulation at  $2^\circ \times 2.5^\circ$ . The GEOS-Chem simulation is driven by  
assimilated meteorological data available from the Goddard Earth Observing System GEOS-5 at the  
NASA GMAO. The model includes a detailed simulation of tropospheric ozone- $\text{NO}_x$ -hydrocarbon  
chemistry as well as of aerosols and their precursors (Bey et al., 2001; Park et al., 2004).

665 The global anthropogenic emissions in this GEOS-Chem simulation are from EDGAR 3.2FT2000  
(Olivier et al., 2001) for 2000, which are scaled to 2005 following van Donkelaar et al. (2008). The  
global inventory is overwritten by the following regional inventories: The US EPA NEI for 2005  
over the United States, the CAC inventory (<http://www.ec.gc.ca/inrp-npri>) for 2005 over Canada,  
the BRAVO inventory (Kuhns et al., 2005) for 1999 over Mexico, the EMEP inventory for 2005  
670 over Europe, the inventory from Zhang et al. (2007) for 2006 over East Asia.  $\text{NO}_x$  emissions from  
soils, lightning, biomass burning, and aircraft are as described in Lamsal et al. (2010, 2011).

The GEOS-Chem simulation of  $\text{NO}_x$  has been evaluated extensively with in situ and satellite  
observations and generally agrees to within 30 % of measured  $\text{NO}_x$  (Martin et al., 2006; Hudman  
et al., 2007; Boersma et al., 2008b). We conducted a simulation for the year 2005 and sample the  
675 model output between 13:00 and 15:00 local time for analysis of the OMI data.

*Acknowledgements.* The work was supported by NASA's Earth Science Division through an Aura Science  
team grant. The Dutch-Finnish-built OMI instrument is part of the NASA EOS Aura satellite payload. The  
OMI instrument is managed by KNMI and the Netherlands Agency for Aero-space Programs (NIVR).

## References

- 680 Bechle, M. J., Millet, D. B., and Marshall, J. D.: Remote sensing of exposure to NO<sub>2</sub>, satellite versus ground-based measurement in a large urban, *Atmos. Environ.*, 69, doi:10.1016/j.atmosenv.2012.11.046, 2013.
- Beirle, S., Platt, U., Wenig, M., and Wagner, T.: Weekly cycle of NO<sub>2</sub> by GOME measurements: a signature of anthropogenic sources, *Atmos. Chem. Phys.*, 3, 2225–2232, 2003.
- Beirle, S., , Boersma, K. F., Platt, U., Lawrence, M. G., and Wagner, T.: Megacity Emissions and Lifetimes of  
685 Nitrogen Oxides Probed from Space, *Science*, 333(6050), 1737–1739, doi:10.1126/science.1207824, 2011.
- Benkovitz, C. M., Scholtz, M. T., Pacyna, J., Terrasón, L., Dignon, J., Voldner, E. C., Spiro, P. A., Logan, J. A., and Graedel, T. E.: Global gridded inventories of anthropogenic emissions of sulfur and nitrogen, *J. Geophys. Res.*, 101, 29 239–29 253, 1996.
- Bey, I., Jacob, D. J., Yantosca, R. M., Logan, J. A., Field, B. D., Fiore, A. M., Li, Q., Liu, H. Y., , Mickley,  
690 L. R., and Schultz, M. G.: Global modeling of tropospheric chemistry with assimilated meteorology: Model description and evaluation, *J. Geophys. Res.*, 106, 23 073–23 096, 2001.
- Blond, N., Boersma, K. F., Eskes, H. J., van der A, R. J., Van Roozendaal, M., De Smedt, I., Bergametti, G., and Vautard, R.: Intercomparison of SCIAMACHY nitrogen dioxide observations, in situ measurements and air quality modeling results over Western Europe, *J. Geophys. Res.*, 112, 10.1029/2006JD007277, 2007.
- 695 Boersma, K. F., Eskes, H. J., and Brinksma, E. J.: Error analysis for tropospheric NO<sub>2</sub> retrieval from space, *J. Geophys. Res.*, 109, doi:10.1029/2003JD003962, 2004.
- Boersma, K. F., Eskes, H. J., Veefkind, J. P., Brinksma, E. J., van der A, R. J., Sneep, M., van den Oord, G. H. J., Levelt, P. F., Stammes, P., Gleason, J. F., and Bucsela, E. J.: Near-real time retrieval of tropospheric NO<sub>2</sub> from OMI, *Atmos. Chem. Phys.*, 112, 2103–2118, 2007.
- 700 Boersma, K. F., Jacob, D. J., Bucsela, E. J., Perring, A. E., Dirksen, R., van der A, R. J., Yantosca, R. M., Park, R. J., Wenig, M. O., Bertram, T. H., and Cohen, R. C.: Validation of OMI tropospheric NO<sub>2</sub> observations during INTEX-B and application to constrain NO<sub>x</sub> emissions over the eastern United States and Mexico, *Atmos. Environ.*, 42, 4480–4497, 2008a.
- Boersma, K. F., Jacob, D. J., Eskes, H. J., Pinder, R. W., Wang, J., and van der A, R. J.: Intercomparison  
705 of SCIAMACHY and OMI tropospheric NO<sub>2</sub> columns: observing the diurnal evolution of chemistry and emissions from space, *J. Geophys. Res.*, 113, doi:10.1029/2007JD008816, 2008b.
- Boersma, K. F., Jacob, D. J., Trainic, M., Rudich, Y., DeSmedt, I., Dirksen, R., and Eskes, H. J.: Validation of urban NO<sub>2</sub> concentrations and their diurnal and seasonal variations observed from space (SCIAMACHY and OMI sensors) using in situ measurements in Israeli cities, *Atmos. Chem. Phys.*, 9, 3867–3879, 2009.
- 710 Boersma, K. F., Eskes, H. J., Dirksen, R. J., van der A, R. J., Veefkind, J. P., et al.: An improved tropospheric NO<sub>2</sub> column retrieval algorithm for the Ozone Monitoring Instrument, *Atmos. Meas. Tech.*, 4, 1905–1928, doi:10.5194/amt-4-1905-2011, 2011.
- Brinksma, E., Pinardi, G., Braak, R., Volten, H., Richter, A., Schonhardt, A., Van Roozendaal, M., Fayt, C., Hermans, C., Dirksen, R., Vlemmix, T., Berkhout, A. J. C., Swart, D. P. J., Oetjen, H., Wittrock, F., Wagner,  
715 T., Ibrahim, O. W., de Leeuw, G., Moerman, M., Curier, R. L., Celarier, E. A., Knap, W. H., Veefkind, J. P., Eskes, H. J., Allaart, M., Rothe, R., Piters, A. J. M., and Levelt, P.: The 2005 and 2006 DANDELIONS NO<sub>2</sub> and Aerosol Intercomparison Campaigns, *J. Geophys. Res.*, 113, doi:10.1029/2007JD008808, 2008.
- Bucsela, E. J., Celarier, E. A., Wenig, M. O., Gleason, J. F., Veefkind, J. P., Boersma, K. F., and Brinksma, E. J.:

- Algorithm for NO<sub>2</sub> vertical column retrieval from the Ozone Monitoring Instrument, *IEEE Trans. Geo. Rem. Sens.*, 44, 1245–1258, 2006.
- 720 Bucsela, E. J., Perring, A. E., Cohen, R. C., Boersma, K. F., Celarier, E. J., Gleason, J. F., Wenig, M. O., Bertram, T. H., Wooldrige, P. J., Dirksen, R., and Veefkind, J. P.: Comparison of NO<sub>2</sub> in situ aircraft measurements with data from the Ozone Monitoring Instrument, *J. Geophys. Res.*, doi:10.1029/2007JD008838, 2008.
- 725 Bucsela, E. J., Pickering, K. E., Huntermann, T. L., et al.: Lightning-generated NO<sub>x</sub> seen by the Ozone Monitoring Instrument during NASA's Tropical Composition, Cloud and Climate Coupling Experiment (TC4), *J. Geophys. Res.*, 115, D00J10, doi:10.1029/2009JD013118, 2010.
- Bucsela, E. J., Krotkov, N. A., Celarier, E. A., Lamsal, L. N., Swartz, W. H., Bhartia, P. K., Boersma, K. F., Veefkind, J. P., Gleason, J. F., and Pickering, K. E.: A new stratospheric and tropospheric NO<sub>2</sub> retrieval  
730 algorithm for nadir-viewing satellite instruments: application to OMI, *Atmos. Meas. Tech.*, 6, 2607–2626, 2013.
- Cede, A., Herman, J., Richter, A., Krotkov, N. A., and Burrows, J. P.: Measurements of nitrogen dioxide total column amounts using a Brewer double spectrophotometer in direct Sun mode, *J. Geophys. Res.*, 111, D05304, doi:10.1029/2005JD006585, 2006.
- 735 Celarier, E. A., Brinksma, E. J., Gleason, J. F., Veefkind, J. P., Cede, A., Herman, J. R., Ionov, D., Goutail, F., Pommereau, J. P., Lambert, J. C., van Roozendaal, M., Pinardi, G., Witrock, F., Schönhardt, A., Richter, A., Ibrahim, O. W., Wagner, T., Bojkov, B., Mount, G., Spinei, E., Chen, C. M., Pongetti, T. J., Sander, S. P., Bucsela, E. J., Wenig, M. O., Swart, D. P. J., Volten, H., Kroon, M., and Levelt, P. F.: Validation of Ozone Monitoring Instrument nitrogen dioxide columns, *J. Geophys. Res.*, 113, doi:10.1029/2007JD008908, 2008.
- 740 de Wildt, M. R., Eskes, H., and Boersma, K. F.: The global economic cycle and satellite-derived NO<sub>2</sub> trends over shipping lanes, *Geophys. Res. Lett.*, 39, 101802, doi:10.1029/2011GL049541, 2012.
- Dobber, M. R., Kleipool, Q., Dirksen, R., Levelt, P. F., Jaross, G., Taylor, S., Kelly, T., Flynn, L., Leppelmeier, G., and Rozemeijer, N.: Validation of Ozone Monitoring Instrument level 1b data products, *J. Geophys. Res.*, 113, doi:10.1029/2007JD008665, 2008.
- 745 Douglass, A. R., Stolarski, R. S., Strahan, S. E., and Connell, P. S.: Radicals and reservoirs in the GMI chemistry and transport model: Comparison to measurements, *J. Geophys. Res.*, 109, D16302, doi:10.1029/2004JD004632, 2004.
- Duncan, B. N., Strahan, S. E., Yoshida, Y., Steenrod, S. D., and Livesey, N.: Model study of the cross-tropopause transport of biomass burning pollution, *Atmos. Chem. Phys.*, 7, 3713–3736, 2007.
- 750 Duncan, B. N., Yoshida, Y., de Foy, B., Lamsal, L. N., Streets, D., Lu, Z., Pickering, K. E., and Krotkov, N. A.: The observed response of the Ozone Monitoring Instrument (OMI) NO<sub>2</sub> column to NO<sub>x</sub> emission controls on power plants in the United States: 2005–2011, *Atmos. Environ.*, 81, 102–111, 2013.
- Edgerton, E. S., Hartsell, B. E., Saylor, R. D., Jansen, J. J., Hansen, D. A., and Hidy, G. M.: The Southeastern Aerosol Research and Characterization Study, part 3: Continuous measurements of fine particulate matter  
755 mass and composition, *J. Air Waste Mgt. Assoc.*, 56(9), 1325–1341, 2006.
- EPA: Primary national ambient air quality standard for nitrogen dioxide, Tech. rep., Environmental Protection Agency, Federal Register, Vol. 74, No. 134, 2009.
- Eskes, H. J. and Boersma, K. F.: Averaging kernels for DOAS total-column satellite retrievals, *Atmos. Chem.*

Phys., 3, 1285–1291, 2003.

- 760 Ghude, S. D., Lal, D. M., Beig, G., et al.: Rain-induced soil NO<sub>x</sub> emission from India during the onset of the summer monsoon: A satellite perspective, *J. Geophys. Res.*, 115, D16304, doi:10.1029/2009JD013367, 2010.
- Ghude, S. D., Pfister, G. G., Jena, C., et al.: Satellite constraints of nitrogen oxide emissions from India based on OMI observations and WRF-Chem simulations, *Geophys. Res. Lett.*, 40, doi:10.1029/2012GL053926, 765 2013a.
- Ghude, S. D., Kulkarni, S. H., Jena, C., Pfister, G. G., Beig, G., Fadnavis, S., and van der A, R. J.: Application of satellite observations for identifying regions of dominant sources of nitrogen oxides over the Indian Subcontinent, *J. Geophys. Res.*, 118, doi:10.1029/2012JD017811, 2013b.
- Hains, J., Boersma, K. F., Kroon, M., et al.: Testing and improving OMI DOMINO tropospheric NO<sub>2</sub> using 770 observations from the DANDELIONS and INTEX-B validation campaigns, *J. Geophys. Res.*, 115, D05301, doi:10.1029/2009JD012399, 2010.
- Heckel, A., Kim, S. W., Frost, G. J., Richter, A., Trainer, M., and Burrows, J. P.: Influence of low spatial resolution a priori data on tropospheric NO<sub>2</sub> satellite retrievals, *Atmos. Meas. Tech.*, 4(9), 1805–1820, doi:10.5194/amt-4-1805-2011, 2011.
- 775 Heland, J., Schlager, H., Richter, A., and Burrows, J. P.: First comparison of tropospheric NO<sub>2</sub> column densities retrieved from GOME measurements and in situ aircraft profile measurements, *Geophys. Res. Lett.*, 29, doi:10.1029/2002GL015528, 2002.
- Herman, J. R., Cede, A., Spinei, E., Mount, G., Tzortziou, M., and Abuhassan, N.: NO<sub>2</sub> column amounts from ground-based Pandora and MFDOAS spectrometers using the direct-sun DOAS technique: Intercomparisons 780 and application to OMI validation, *J. Geophys. Res.*, 114, D13307, doi:10.1029/2009JD011848, 2009.
- Herron-Thorpe, F. L., Lamb, B. K., Mount, G. H., and Vaughan, J. K.: Evaluation of a regional air quality forecast model for tropospheric NO<sub>2</sub> columns using the OMI/Aura satellite tropospheric NO<sub>2</sub> product, *Atmos. Chem. Phys.*, 10, 8839–8854, doi:10.5194/acp-10-8839-2010, 2010.
- Hilboll, A., Richter, A., and Burrows, J. P.: Long-term changes of tropospheric NO<sub>2</sub> over megacities derived 785 from multiple satellite instruments, *Atmos. Chem. Phys.*, 13, 4145–4169, doi:10.5194/acp-13-4145-2013, 2013.
- Hirsch, R. M. and Gilroy, E. J.: Methods of fitting a straight line to data: Examples in water resources, *Water Res. Bull.*, 20(5), 705–711, 1984.
- Hönninger, G., von Friedeburg, C., and Platt, U.: Multi axis differential optical absorption spectroscopy (MAX- 790 DOAS), *Atmos. Chem. Phys.*, 4, 231–254, doi:10.5194/acp-4-231-2004, 2004.
- Hudman, R. C., Jacob, D. J., Turquety, S., Leibensperger, E. M., Murray, L. T., Wu, S., Gilliland, A. B., Avery, M., Bertram, T. H., Brune, W., Cohen, R. C., Dibb, J. E., Flocke, F. M., Fried, A., Holloway, J., Neuman, J. A., Orville, R., Perring, A., Ren, X., Sachse, G. W., Singh, H. B., Swanson, A., and Wooldridge, P. J.: Surface and lightning sources of nitrogen oxides over the United States: magnitudes, chemical evolution, 795 and outflow, *J. Geophys. Res.*, 112, doi:10.1029/2006JD007912, 2007.
- Huijnen, V., Eskes, H. J., Poupkou, A., et al.: Comparison of OMI NO<sub>2</sub> tropospheric columns with an ensemble of global and European regional air quality models, *Atmos. Chem. Phys.*, 10, 3273–3296, 2010.
- Intergovernmental Panel on Climate Change (IPCC): Contribution of working group I to the Fourth Assessment

- Report of the Intergovernmental Panel on Climate Change, in: *Climate Change 2007: The Physical Science Basis*, edited by Solomon et al., p. 996, Cambridge University Press, Cambridge, United Kingdom, 2007.
- 800 Ionov, D. V., Timofeyev, Y. M., Sinyakov, V. P., Semenov, V. K., Goutail, F., Pommereau, J. P., Bucsel, E. J., Celarier, E. A., and Kroon, M.: Ground-based validation of EOS-Aura OMI NO<sub>2</sub> vertical column data in the midlatitude mountain ranges of Tien Shan (Kyrgyzstan) and Alps (France), *J. Geophys. Res.*, 113, doi:10.1029/2007JD008659, 2008.
- 805 Irie, H., Kanaya, Y., Akimoto, H., Tanimoto, H., Z. Wang, J. F. G., and Bucsel, E. J.: Validation of OMI tropospheric NO<sub>2</sub> column data using MAX-DOAS measurements deep inside the North China Plain in June 2006: Mount Tai Experiment 2006, *Atmos. Chem. Phys.*, 8, 6577–6586, doi:10.5194/acp-8-6577-2008, 2008.
- Irie, H., Boersma, K. F., Kanaya, Y., Takashima, H., Pan, X., and Wang, Z. F.: Quantitative bias estimates for 810 tropospheric NO<sub>2</sub> columns retrieved from SCIAMACHY, OMI, and GOME-2 using a common standard for East Asia, *Atmos. Meas. Tech.*, 5, 2403–2411, doi:10.5194/amt-5-2403-2012, 2012.
- Jaeglé, L., Steinberger, L., Martin, R. V., and Chance, K.: Global partitioning of NO<sub>x</sub> sources using satellite observations: Relative roles of fossil fuel combustion, biomass burning and soil emissions, *Faraday Discussions*, 130, doi: 10.1039/b502128f, 2005.
- 815 Kim, S. W., Heckel, A., McKeen, S. A., Frost, G. J., Hsie, E. Y., Trainer, M. K., Richter, A., Burrows, J. P., Peckham, S. E., and Grell, G. A.: Satellite-observed U.S. power plant NO<sub>x</sub> emission reductions and their impact on air quality, *Geophys. Res. Lett.*, 33, L22812, doi:10.1029/2006GL027749, 2006.
- Kim, S. W., Heckel, A., Frost, G. J., Richter, A., Gleason, J., Burrows, J. P., McKeen, S. A., Hsie, E. Y., 820 Granier, C., and Trainer, M. K.: NO<sub>2</sub> columns in the western United States observed from space and simulated by a regional chemistry model and their implications for NO<sub>x</sub> emissions, *J. Geophys. Res.*, 114, D11301, doi:10.1029/2008JD011343, 2009.
- Knepp, T., Pippin, M., Crawford, J., Chen, G., Szykman, J., Long, R., Cowen, L., Cede, A., Abuhassan, N., Herman, J., Delgado, R., Compton, J., Berkoff, T., Fishman, J., Martins, D., Stauffer, R., Thompson, A. M., Weinheimer, A., Knapp, D., Montzka, D., Lenschow, D., and Neil, D.: Estimating surface NO<sub>2</sub> and 825 SO<sub>2</sub> mixing ratios from fast-response total column observations and potential application to geostationary missions, *J. Atmos. Chem.*, DOI 10.1007/s10874-013-9257-6, 2013.
- Konovalov, I. B., Beekmann, M., Richter, A., and Burrows, J. P.: Inverse modelling of the spatial distribution of NO<sub>x</sub> emissions on a continental scale using satellite data, *Atmos. Chem. Phys.*, 6, 1747–1770, 2006.
- Kramer, L. J., Leigh, R. J., Remedios, J. J., and Monks, P. S.: Comparison of OMI and ground-based in situ 830 and MAX-DOAS measurements of tropospheric nitrogen dioxide in an urban area, *J. Geophys. Res.*, 113, doi:10.1029/2007JD009168, 2008.
- Kuhns, H., Knipping, E. M., and Vokovich, J. M.: Development of a United States-Mexico emissions inventory for the Big Bend Regional Aerosol and Visibility Observational (BRAVO) study, *J. Air Waste Mgt. Assoc.*, 55, 677–692, 2005.
- 835 Lamsal, L. N., Martin, R. V., van Donkelaar, A., Steinbacher, M., Celarier, E. A., Bucsel, E., Dunlea, E. J., and Pinto, J. P.: Ground-level nitrogen dioxide concentrations inferred from the satellite-borne Ozone Monitoring Instrument, *J. Geophys. Res.*, 113, D16308, doi:10.1029/2007JD009235, 2008.
- Lamsal, L. N., Martin, R. V., van Donkelaar, A., Celarier, E. A., Bucsel, E. J., Boersma, K. F., Luo, R.



- D. C., and Wang, Y.: Indirect validation of tropospheric nitrogen dioxide retrieved from the OMI satellite instrument: Insight into the seasonal variation of nitrogen oxides at northern midlatitudes, *J. Geophys. Res.*, 115, D05302, doi:10.1029/2009JD013351, 2010.
- Lamsal, L. N., Martin, R. V., Padmanabhan, A., van Donkelaar, A., Zhang, Q., Sioris, C. E., Chance, K., Kurosu, T. P., and Newchurch, M. J.: Application of satellite observations for timely updates to global anthropogenic NO<sub>x</sub> emission inventories, *Geophys. Res. Lett.*, 38, L05810, doi:10.1029/2010GL046476, 2011.
- 845 Lamsal, L. N., Martin, R. V., Parrish, D. D., and Krotkov, N. A.: Scaling relationship for NO<sub>2</sub> pollution and population size: A satellite perspective, *Environ. Sci. Technol.*, 47, 7855–7861, 2013.
- Leitão, J., Richter, A., Vrekoussis, M., Kokhanovsky, A., Zhang, Q. J., Beekmann, M., and Burrows, J. P.: On the improvement of NO<sub>2</sub> satellite retrievals aerosol impact on the air mass factors, *Atmos. Meas. Tech.*, 3, 475–493, 2010.
- 850 Levelt, P. F., van den Oord, G. H. J., Dobber, M. R., Malkki, A., Visser, H., de Vries, J., Stammes, P., Lundell, J. O. V., and Saari, H.: The Ozone Monitoring Instrument, *IEEE Trans. Geo. Rem. Sens.*, 44, 1093–1101, 2006.
- Lin, J. T.: Satellite constraint for emissions of nitrogen oxides from anthropogenic, lightning and soil sources over East China on a high-resolution grid, *Atmos. Chem. Phys.*, 12, 2881–2898, doi:10.5194/acp-12-2881-2012, 2012.
- 855 Lin, J. T., McElroy, M. B., and Boersma, K. F.: Constraint of anthropogenic NO<sub>x</sub> emissions in China from different sectors: a new methodology using multiple satellite retrievals, *Atmos. Chem. Phys.*, 10, 63–78, 2010.
- Lu, Z. and Streets, D. G.: Increase in NO<sub>x</sub> emissions from Indian thermal power plants during 1996–2010: Unit-based inventories and multisatellite observations, *Environ. Sci. Technol.*, 46, 7463–7470, doi:10.1021/es300831w, 2012.
- Martin, R. V., Chance, K., Jacob, D. J., et al.: An improved retrieval of tropospheric nitrogen dioxide from GOME, *J. Geophys. Res.*, 107, doi:10.1029/2001JD001027, 2002.
- Martin, R. V., Jacob, D. J., Chance, K., Kurosu, T. P., Perner, P. I., and Evans, M. J.: Global inventory of nitrogen oxide emission constrained by space-based observations of NO<sub>2</sub> columns, *J. Geophys. Res.*, 108, doi:10.1029/2003JD003453, 2003.
- 865 Martin, R. V., Sioris, C. E., Chance, K., Ryerson, T. B., Bertram, T. H., Wooldridge, P. J., Cohen, R. C., Neuman, J. A., Swanson, A., and Flocke, F. M.: Evaluation of space-based constraints on global nitrogen oxide emissions with regional aircraft measurements over and downwind of eastern North America, *J. Geophys. Res.*, 111, doi:10.1029/2005JD006680, 2006.
- 870 McLinden, C. A., Fioletov, V., Boersma, K. F., Kharol, S. K., Krotkov, N. A., Lamsal, L. N., Makar, P. A., Martin, R. V., Veefkind, J. P., and Yang, K.: Improved satellite retrievals of NO<sub>2</sub> and SO<sub>2</sub> over the Canadian oil sands and comparisons with surface measurements, *Atmos. Chem. Phys.*, 14, doi:10.5194/acp-14-3637-2014, 2014.
- Mebust, A. K. and Cohen, R. C.: Observations of a seasonal cycle in NO<sub>x</sub> emissions from fires in African woody savannas, *Geophys. Res. Lett.*, 40, 1451–1455, doi:10.1002/grl.50343, 2013.
- Mebust, A. K., Russell, A. R., Hudman, R. C., Valin, L. C., and Cohen, R. C.: Characterization of wildfire NO<sub>x</sub> emissions using MODIS fire radiative power and OMI tropospheric NO<sub>2</sub> columns, *Atmos. Chem. Phys.*,

11(12), 5839–5851, doi:10.5194/acp-11-5839-2011, 2011.

- 880 NARSTO: Improving emission inventories for effective air quality management across North America, A  
NARSTO Assessment, Tech. rep., NARSTO, <http://www.narsto.org/>, NARSTO-05-001, 2005.
- Novotny, E. V., Bechle, M. J., Millet, D. B., and Marshal, J. D.: National satellite-based land-use regression:  
NO<sub>2</sub> in the United States, *Environ. Sci. Technol.*, 45(10), 4407–4414, doi:10.1021/es103578x, 2011.
- O’Byrne, G., Martin, R. V., van Donkelaar, A., Joiner, J., and Celarier, E. A.: Surface reflectivity from OMI  
885 using MODIS to eliminate clouds: effects of snow on UV-Vis trace gas retrievals, *J. Geophys. Res.*, 115,  
D17305, doi:10.1002/jdrd.50550, 2010.
- Oetjen, H., Baidar, S., Krotkov, N. A., Lamsal, L. N., Lechner, M., and Volkamer, R.: Airborne MAX-DOAS  
measurements over California: Testing the NASA OMI tropospheric NO<sub>2</sub> product, *J. Geophys. Res.*, 118,  
13, doi:10.1002/jdrd.50550, 2013.
- 890 Olivier, J. G. J., Berdowski, J. J. M., Peters, J. A. H. W., Bakker, J., Visschedijk, A. J. H., and Bloos, J. P. J.:  
Applications of EDGAR. Including a description of EDGAR 3.2 : Reference database with trend data for  
1970–1995, Tech. rep., RIVM Bilthovan, RIVM report, 773301 001/NRP report 410200 051, 2001.
- Palmer, P. I., Jacob, D. J., Chance, K., Martin, R. V., Kurosu, T. P., Bey, I., Yantosca, R., Fiore, A. M., and Li, Q.:  
Air mass factor formulation for spectroscopic measurements from satellites: Application to formaldehyde  
895 retrievals from the Global Ozone Monitoring Experiment, *J. Geophys. Res.*, 106, 14 539–14 550, 2001.
- Palmer, P. I., Jacob, D. J., Fiore, A. M., Martin, R. V., Chance, K., and Kurosu, T. P.: Mapping isoprene  
emissions over North America using formaldehyde column observations from space, *J. Geophys. Res.*, 108,  
doi:10.1029/2002JD002153, 2003.
- Park, R. J., Jacob, D. J., Field, B. D., Yantosca, R. M., and Chin, M.: Natural and transboundary pollution  
900 influences on sulfate-nitrate-ammonium aerosols in the United States: implications for policy, *J. Geophys.  
Res.*, 109, 10.1029/2003JD004473, 2004.
- Piters, A. J. M. et al.: Cabauw intercomparison campaign for nitrogen dioxide measuring instruments (CINDI):  
design, execution, and early results, *Atmos. Meas. Tech.*, 5, 457–485, doi:10.5194/amt-5-457-2012, 2012.
- Platt, U.: Differential Optical Absorption Spectroscopy (DOAS), in: *Air Monitoring by Spectroscopic Tech-  
905 niques*, edited by Sigrist, M. W., pp. 27–84, John Wiley, New York, USA, 1994.
- Richter, A., Burrows, J. P., Nüß, H., Granier, C., and Niemeier, U.: Increase in tropospheric nitrogen dioxide  
levels over China observed from space, *Nature*, 437, 129–132, 2005.
- Ridley, B., Ott, L., Pickering, K., Emmons, L., Montzka, D., Weinheimer, A., Knapp, D., Grahek, F., Li,  
L., Heymsfield, G., McGill, M., Kucera, P., Mahoney, M. J., Schultz, M., and Brasseur, G.: Florida thun-  
910 derstorms: A faucet of reactive nitrogen to the upper troposphere, *J. Geophys. Res.*, 109, D17305, doi:  
10.1029/2004JD004769, 2004.
- Ridley, B. A. and Grahek, F.: A small, low flow, high-sensitivity reaction vessel for NO chemiluminescence  
detectors, *J. Atmos. Ocean. Tech.*, 7, 307–311, 1990.
- Roscoe, H. K. et al.: Intercomparison of slant column measurements of NO<sub>2</sub> and O<sub>4</sub> by MAX-DOAS and  
915 zenith-sky UV and visible spectrometers, *Atmos. Meas. Tech.*, 3, 1629–1646, doi:10.5194/amt-3-1629-2010,  
2010.
- Russell, A. R., Perring, A. E., Valin, L. C., Bucsela, E. J., Browne, E. C., Wooldridge, P. J., and Cohen, R. C.: A  
high spatial resolution retrieval of NO<sub>2</sub> column densities from OMI: method and evaluation, *Atmos. Chem.*

- Phys., 11, 8543–8554, doi:10.5194/acp-11-8543-2011, 2011.
- 920 Russell, A. R., Valin, L. C., and Cohen, R. C.: Trends in OMI NO<sub>2</sub> observations over the United States: effects of emission control technology and the economic recession, *Atmos. Chem. Phys.*, 12, 12 197–12 209, doi:10.5194/acp-12-12197-2012, 2012.
- Russell, A. R. et al.: Space-based Constraints on Spatial and Temporal Patterns of NO<sub>x</sub> Emissions in California, 2005-2008, *Environ. Sci. Technol.*, 44(9), 3608–3615, doi:10.1021/es903451j, 2010.
- 925 Ryerson, T. B., Williams, E. J., and Fehsenfeld, F. C.: An efficient photolysis system for fast-response NO<sub>2</sub> measurements, *J. Geophys. Res.*, 105, 26 447–26 461, 2000.
- Schaub, D., Boersma, K. F., Kaiser, J. W., Weiss, A. K., Folini, D., Eskes, H. J., and Buchmann, B.: Comparison of GOME tropospheric NO<sub>2</sub> columns with NO<sub>2</sub> profiles deduced from ground-based in situ measurements, *Atmos. Chem. Phys.*, 6, 3211–3229, 2006.
- 930 Schaub, D., Brunner, D., Boersma, K. F., Keller, J., Folini, D., Buchmann, B., Berresheim, H., and Staehelin, J.: SCIAMACHY tropospheric NO<sub>2</sub> over Switzerland: estimates of NO<sub>2</sub> lifetimes and impact of the complex Alpine topography on the retrieval, *Atmos. Chem. Phys.*, 7, 5971–5987, 2007.
- Solomon, S., Portmann, R. W., Sanders, R. W., Daniel, J. S., Madsen, W., Bartram, B., and Dutton, E. G.: On the role of nitrogen dioxide in the absorption of solar radiation, *J. Geophys. Res.*, 104(D10), 12 047–12 058, 1999.
- 935 Steinbacher, M., Zellweger, C., Schwarzenbach, B., Bugmann, S., Buchmann, B., Ordóñez, C., Prévôt, A. S. H., and Hueglin, C.: Nitrogen oxides measurements at rural sites in Switzerland: Bias of conventional measurement techniques, *J. Geophys. Res.*, 10.1029/2006JD007971, 2007.
- Strahan, S. E., Duncan, B. N., and Hoor, P.: Observationally derived transport diagnostics for the lowermost stratosphere and their application to the GMI chemistry and transport model, *Atmos. Chem. Phys.*, 7, 2435–2445, 2007.
- Streets, D. G., Zhang, Q., Wang, L., He, K., Hao, J., Wu, Y., Tang, Y., and Carmichael, G. R.: Revisiting China's CO emissions after the Transport and Chemical Evolution over the Pacific (TRACE-P) mission: Synthesis of inventories, atmospheric modeling, and observations, *J. Geophys. Res.*, doi:10.1029/2006JD007118, 2006.
- 945 Tang, W., Cohan, D., Lamsal, L. N., Xiao, X., and Zhou, W.: Inverse modeling of Texas NO<sub>x</sub> emissions using space-based and ground-based NO<sub>2</sub> observations, *Atmos. Chem. Phys.*, 13, 11 005–11 018, 2013.
- Thornton, J. A., Wooldridge, P. J., and Cohen, R. C.: Atmospheric NO<sub>2</sub>: in situ laser-induced fluorescence detection at parts per trillion mixing ratios, *Anal. Chem.*, 72, 528, 2000.
- Toenges-Schüller, N., Stein, O., Rohrer, F., Wahner, A., Richter, A., Burrows, J. P., Beirle, S., Wagner, T., Platt, U., and Elvidge, C. D.: Global distribution pattern of anthropogenic nitrogen oxide emissions: Correlation analysis of satellite measurements and model calculations, *J. Geophys. Res.*, doi:10.1029/2005JD006068, 2006.
- 950 Valin, L. C., Russell, A. R., Hudman, R. C., and Cohen, R. C.: Effects of model spatial resolution on the interpretation of satellite NO<sub>2</sub> observations, *Atmos. Chem. Phys.*, 11, 11 647–11 655, 2011.
- 955 van der A, R. J., Peters, D. H. M., Eskes, H., Boersma, K. F., Van Roozendael, M., De Smedt, I., and Kelder, H. M.: Detection of the trend and seasonal variation in tropospheric NO<sub>2</sub> over China, *J. Geophys. Res.*, 111, doi:10.1029/2005JD006594, 2006.
- van der A, R. J., Eskes, H. J., Boersma, K. F., van Noije, T. P. C., Van Roozendael, M., De Smedt, I., Peters,

- D. H. M., Kuenen, J. J. P., and Meijer, E. W.: Identification of NO<sub>2</sub> sources and their trends from space using seasonal variability analyses, *J. Geophys. Res.*, 113, doi:10.1029/2007JD009021, 2008.
- 960 van Donkelaar, A., Martin, R. V., Leaitch, W. R., Macdonald, A. M., Walker, T. W., Streets, D. G., Zhang, Q., Dunlea, E. J., Jimenez, J. L., Dibb, J. E., Huey, L. G., Weber, R., and Andreae, M. O.: Analysis of aircraft and satellite measurements from the Intercontinental Chemical Transport Experiment (INTEX-B) to quantify long-range transport of East Asian sulfur to Canada, *Atmos. Chem. Phys.*, 8, 2999–3014, 2008.
- 965 van Donkelaar, A., Martin, R. V., Pasch, A. N., Szykman, J. J., Zhang, L., Wang, Y., and Chen, D.: Improving the accuracy of daily satellite-derived ground-level fine aerosol concentration estimates for North America, *Environ. Sci. Technol.*, 46, 11 971–11 978, dx.doi.org/10.1021/es3025319, 2012.
- van Noije, T. P. C., Eskes, H. J., Dentener, F. J., Stevenson, D. S., Ellingsen, K., Schultz, M. G., Wild, O., Amann, M., Atherton, C. S., Bergmann, D. J., Bey, I., Boersma, K. F., Butler, T., Cofala, J., Drevet, J., 970 Fiore, A. M., Gauss, M., Hauglustaine, D. A., Horowitz, L. W., Isaksen, I. S. A., Krol, M. C., Lamarque, J. F., Lawrence, M. G., Martin, R. V., Montanaro, V., Müller, J. F., Pitari, G., Prather, M. J., Pyle, J. A., Richter, A., Rodriguez, J. M., Savage, N. H., Strahan, S. E., Sudo, K., Szopa, S., and van Roozendaal, M.: Multi-model ensemble simulations of tropospheric NO<sub>2</sub> compared with GOME retrievals for the year 2000, *Atmos. Chem. Phys.*, 6, 2943–2979, 2006.
- 975 Vandaele, A. C., Hermans, C., Simon, P. C., Carleer, M., Colin, R., Fally, S., Merienne, M. F., Jenouvrier, A., and Coquart, B.: Measurements of the NO<sub>2</sub> absorption cross-section from 42000 cm<sup>-1</sup> to 10000 cm<sup>-1</sup> (238–1000 nm) at 220 K and 294 K, *J. Quant. Spectrosc. Rad. Transfer*, 59(3–5), 171–184, 1998.
- Vinken, G. C. M., Boersma, K. F., van Donkelaar, A., and Zhang, L.: Constraints on ship NO<sub>x</sub> emissions in Europe using GEOS-Chem and OMI satellite NO<sub>2</sub> observations, *Atmos. Chem. Phys.*, 14, 1353–1369, 980 doi:10.5194/acp-14-1353-2014, 2014.
- Wagner, N. L., Dubé, W. P., Washenfelder, R. A., Young, C. J., Pollack, I. B., Ryerson, T. B., and Brown, S. S.: Diode laser-based cavity ring-down instrument for NO<sub>3</sub>, N<sub>2</sub>O<sub>5</sub>, NO, NO<sub>2</sub> and O<sub>3</sub> from aircraft, *Atmos. Meas. Tech.*, 4, 1227–1240, doi:10.5194/amt-4-1227-2011, 2011.
- Wang, S., Pongetti, T. J., Sander, S. P., Spinei, E., Mount, G. H., Cede, A., and Herman, J.: Direct sun measurements of NO<sub>2</sub> column abundances from Table Mountain, California: Intercomparison of low- and high- 985 resolution spectrometers, *J. Geophys. Res.*, 115, d13305, doi:10.1029/2009JD013503, 2010.
- Wang, S. W., Zhang, Q., Streets, D. G., He, K. B., Martin, R. V., Lamsal, L. N., Chen, D., Lei, Y., and Lu, Z.: Growth in NO<sub>x</sub> emissions from power plants in China: bottom-up estimates and satellite observations, *Atmos. Chem. Phys.*, 12, 4429–4447, doi:10.5194/acp-12-4429-2012, 2012.
- 990 Wenig, M. O., Cede, A. M., Bucsel, E. J., Celarier, E. A., Boersma, F. K., Veefkind, J. P., Brinksma, E. J., Gleason, J. F., and Herman, J. R.: Validation of OMI tropospheric NO<sub>2</sub> column densities using direct-sun mode Brewer measurements at NASA Goddard Space Flight Center, *J. Geophys. Res.*, 113, D16, doi:10.1029/2007JD008988, 2008.
- Zhang, L., Jacob, D. J., Smith-Downey, N. V., Wood, D. A., Blewitt, D., Carouge, C., van Donkelaar, A., 995 Jones, D. B. A., Murray, L. T., and Wang, Y.: Improved estimate of the policy-relevant background ozone in the United States using the GEOS-Chem global model with 1/2° × 2/3° horizontal resolution over North America, *Atmos. Environ.*, 45, 6769–6776, 2011.
- Zhang, Q., Streets, D. G., He, K., Wang, Y., Richter, A., Burrows, J. P., Uno, I., Jang, C. J., Chen, D., Yao, Z.,

**Table 1.** Aircraft flight parameters.

Site	Location type	Spirals	Minimum and maximum altitude (km)	Number of observations
Beltsville	suburban	43	0.24–2.03	19 867
Padonia	suburban	38	0.35–3.47	27 106
Fair Hill	rural	41	0.26–4.78	41 550
Aldino	rural/suburban	36	0.27–4.82	30 407
Edgewood	coastal/suburban	43	0.25–4.82	35 050
Essex	coastal/urban	38	0.24–3.26	30 269

- and Lei, Y.:  $\text{NO}_x$  emission trends for China, 1995-2004: The view from the ground and the view from space, *J. Geophys. Res.*, 112, doi:10.1029/2007JD008684, 2007.
- Zhao, C. and Wang, Y.: Assimilation inversion of  $\text{NO}_2$  emissions over east Asia using OMI  $\text{NO}_2$  column measurements, *Geophys. Res. Lett.*, 36, L06805, doi:10.1029/2008GL037129, 2009.
- Zhou, Y., Brunner, D., Boersma, K. F., Dirksen, R., and Wang, P.: An improved tropospheric  $\text{NO}_2$  retrieval for OMI observations in the vicinity of mountainous terrain, *Atmos. Meas. Tech.*, 2, 401–416, 2009.

**Table 2.** Summary of validation results.

Location	Data sources	Measurement period	Mean difference	Sample size
Beltsville, MD	P-3B	Jul 2011	-6.0%	8
	Pandora		-5.9%	8
Padonia, MD	P-3B	Jul 2011	-8.0%	9
	Pandora		9.1%	8
Fair Hill, MD	P-3B	Jul 2011	-22.1%	8
	Pandora		43.9%	8
Aldino, MD	P-3B	Jul 2011	-19.5%	8
	Pandora		-5.4%	7
Edgewood, MD	P-3B	Jul 2011	-41.3%	10
	Pandora		-5.8%	8
Essex, MD	P-3B	Jul 2011	-40.1%	13
	Pandora		13.1%	8
Hampton, VA	Pandora	2009–2011	-16.8%	163
Tsukuba, Japan	MAX-DOAS	2006–2007, 2010–2011	-16.3%	191
Hedo, Japan	MAX-DOAS	2007–2011	7.1%	514
Yorkville, GA	In situ surface	2006–2009	-1.9%	700
Centerville, AL	In situ surface	2006–2009	-17.8%	676
Continental USA	NO <sub>x</sub> emission inventory	2005	8.8%	2706

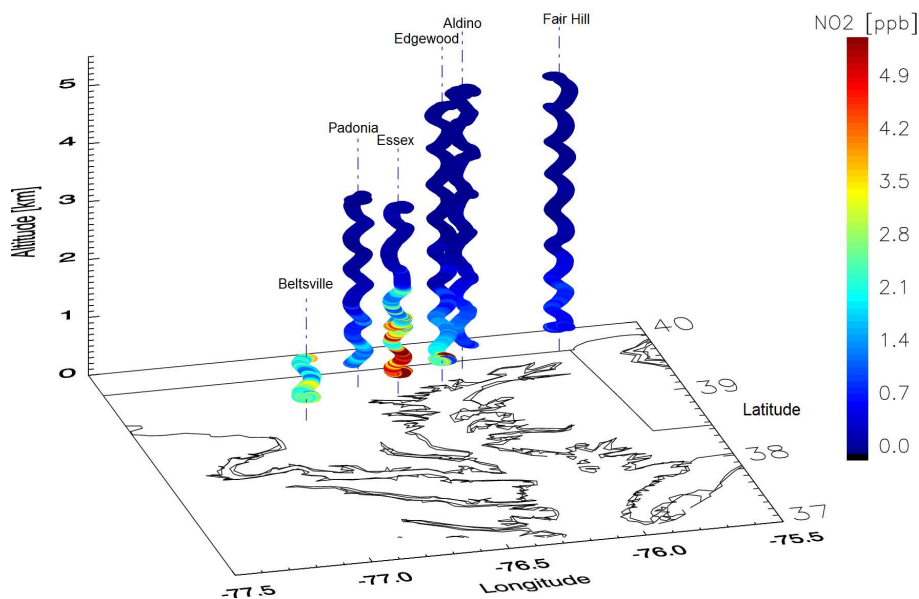


**Fig. 1.** Distribution of NO<sub>2</sub> on 21 July 2011 obtained from P-3B aircraft measurements during the DISCOVER-AQ field campaign in Maryland. More than 190 000 1 s NO<sub>2</sub> measurements were taken during 254 spirals over the entire campaign period.

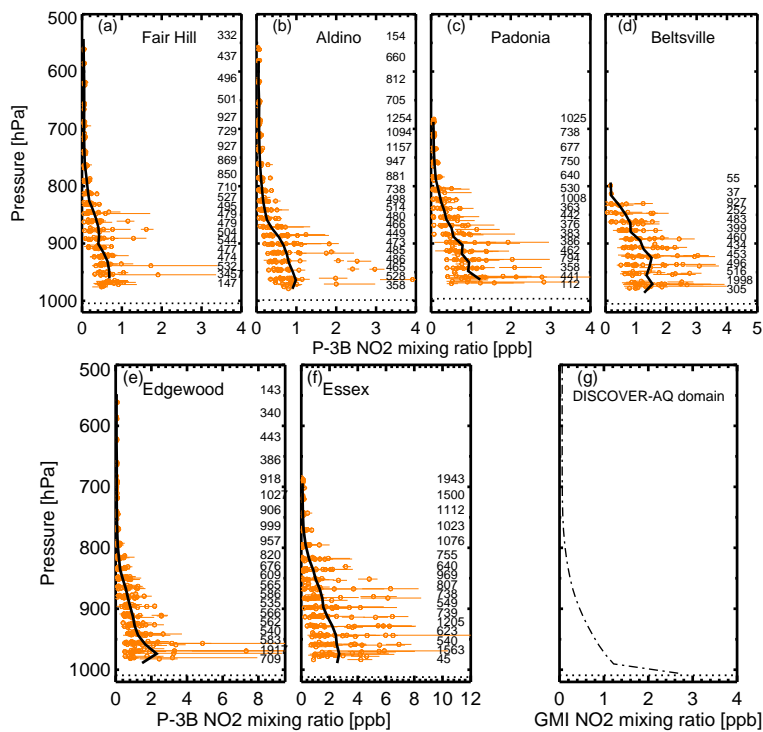


**Fig. 2.** Early afternoon (12:00 to 15:00) vertical mean profile of NO<sub>2</sub> mixing ratio over Fair Hill, Aldino, Padonia, Beltsville, Edgewood, and Essex in Maryland. The open circles (in orange) represent NO<sub>2</sub> mixing ratios averaged over the GMI pressure grid from each spiral. Error bars represent the 10th to 90th percentiles. Solid black lines connect the mean mixing ratios determined from in situ measurements during the entire campaign. The number of measurements within each GMI pressure grid is shown in the right of each panel. The dotted lines show the surface pressure levels. The bottom-right panel shows the GMI a priori monthly (July) mean NO<sub>2</sub> mixing ratio profile over the DISCOVER-AQ domain.

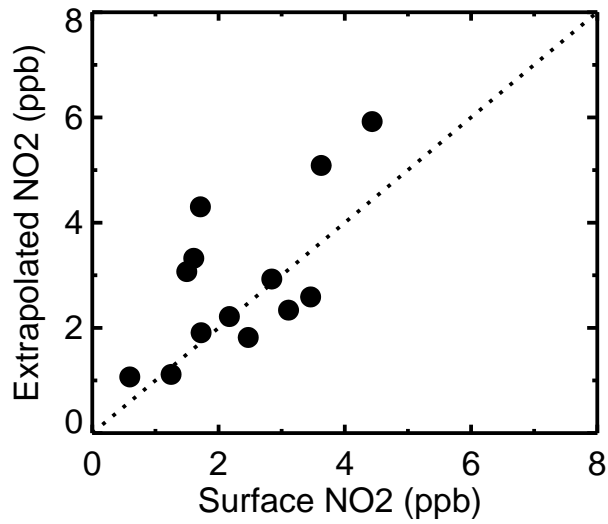


**Fig. 3.** Comparison of aircraft-measured NO<sub>2</sub> profiles extrapolated to the surface (using Eqn. 1) with surface NO<sub>2</sub> measurements with photolytic converter instrument at Padonia during the DISCOVER-AQ field campaign.

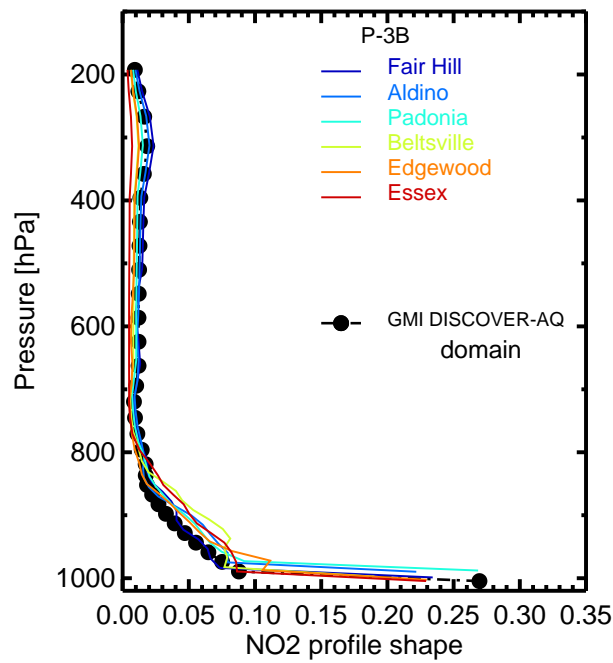


**Fig. 4.** Relative vertical distribution (profile shape) of NO<sub>2</sub> over the six spiral locations during DISCOVER-AQ. The colored lines show the mean profile shapes determined from the in situ measurements. The shape factors are calculated as the ratio of partial columns to total tropospheric column. The dashed line with filled circles shows the profile shape calculated from the GMI model.



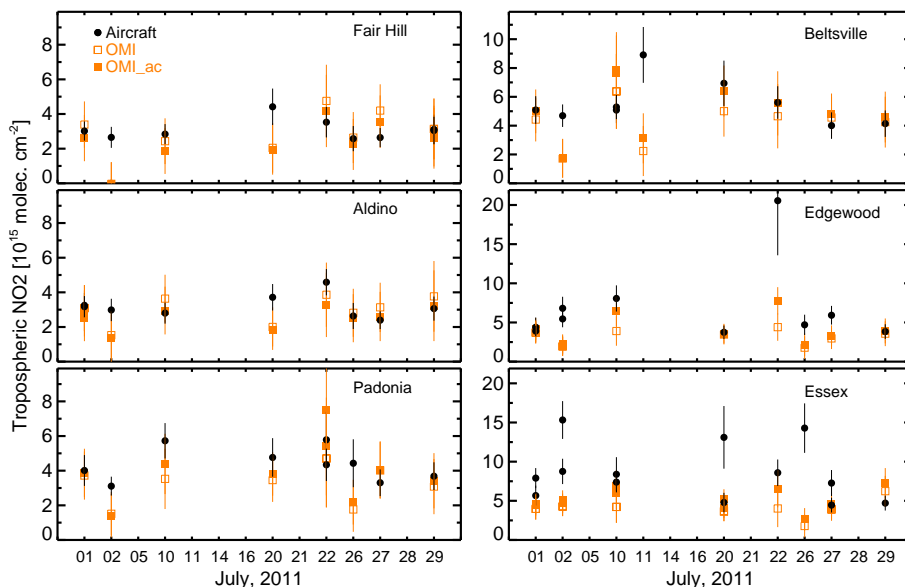


**Fig. 5.** Comparison of tropospheric  $\text{NO}_2$  columns retrieved from OMI (squares) with those determined from in situ measurements (filled circles). The figure shows OMI retrievals performed using GMI  $\text{NO}_2$  a priori vertical profiles (open squares) and in situ  $\text{NO}_2$  measurements (filled squares). Error bars represent errors in the aircraft measurements, extrapolated aircraft profiles, and OMI retrievals.

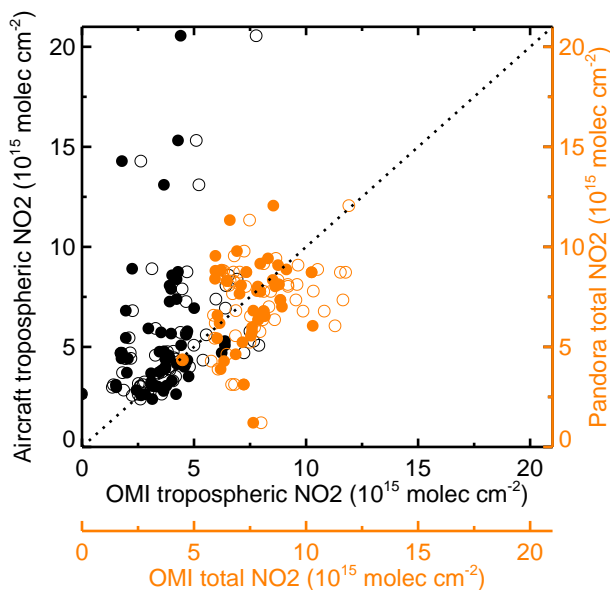


**Fig. 6.** A summary plot showing comparison of collocated tropospheric (black) and total (orange)  $\text{NO}_2$  columns derived from in situ aircraft measurements and retrieved from Pandora with OMI retrievals performed using GMI  $\text{NO}_2$  a priori vertical profiles (filled circles) and in situ  $\text{NO}_2$  measurements (open circles). The dotted line represents the 1:1 relationship.

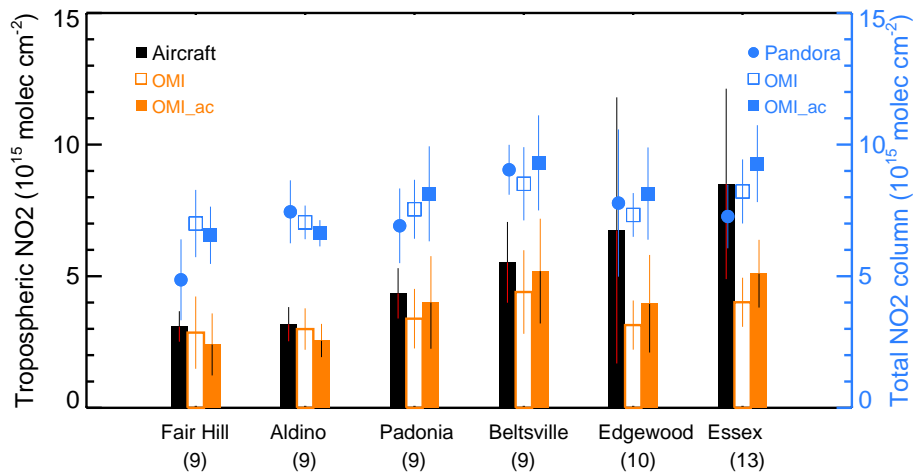


**Fig. 7.** Comparison of average tropospheric (orange bars) and total (blue squares) NO<sub>2</sub> columns retrieved from OMI with tropospheric NO<sub>2</sub> columns determined from in situ aircraft (black bars) measurements and total columns retrieved from Pandora (filled blue circles) at the six locations in Maryland during the DISCOVER-AQ field campaign. Open bars and squares represent the operational retrievals and filled bars and squares represent the retrievals performed using collocated aircraft-measured NO<sub>2</sub> vertical profiles. The vertical lines represent the standard deviation of the average.

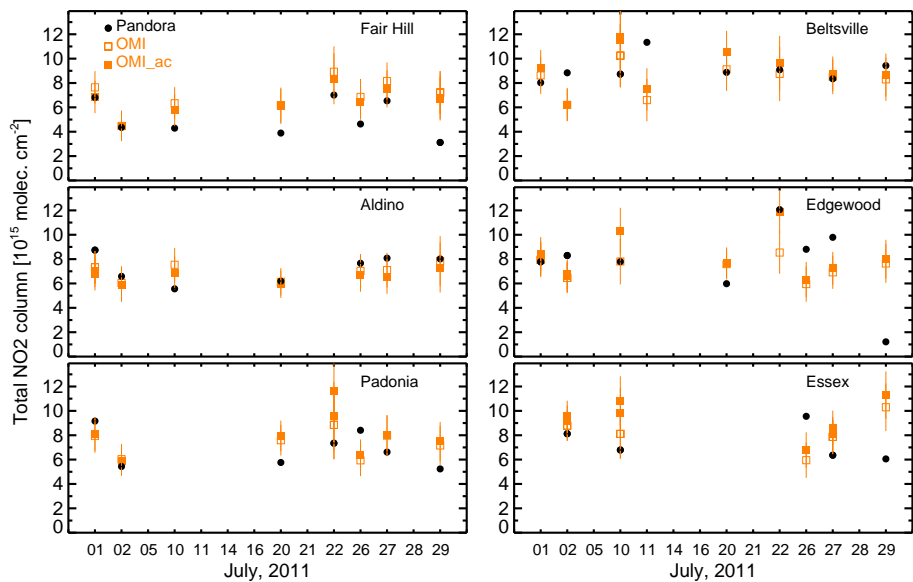


**Fig. 8.** Comparison of total NO<sub>2</sub> columns retrieved from OMI (rectangles) with those retrieved from Pandora measurements (filled circles). Open squares represent the operational retrievals (using GMI profiles), and filled squares represent OMI retrievals performed using collocated aircraft-measured NO<sub>2</sub> vertical profiles. Error bars represent errors in Pandora and OMI retrievals.

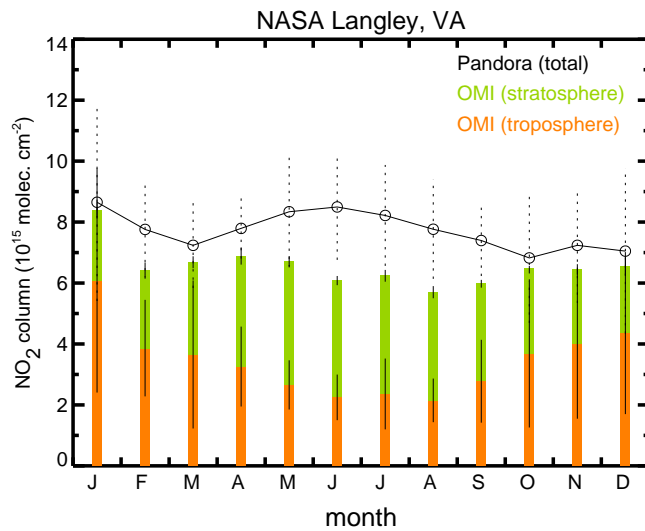


**Fig. 9.** Monthly variation of total  $\text{NO}_2$  columns at Hampton, VA for 2009–2012, as calculated from Pandora measurements (line with open circles) and OMI measurements (bars). OMI total  $\text{NO}_2$  columns are separated into stratospheric (green bars) and tropospheric (orange bars) components. The bars represent the standard deviation of the average.

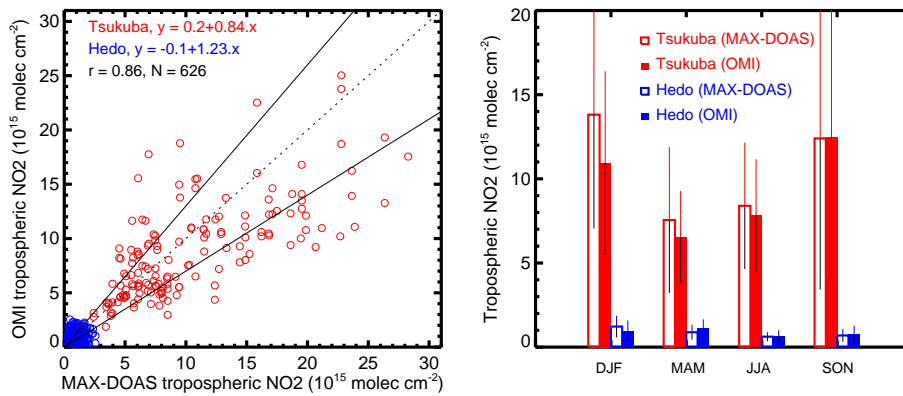


**Fig. 10.** Comparison of tropospheric  $\text{NO}_2$  columns retrieved from OMI and MAX-DOAS instruments. Observations at Tsukuba and Hedo, Japan, are shown in red and blue, respectively. (left) Scatter plot of OMI tropospheric  $\text{NO}_2$  and MAX-DOAS measurements. The regression analysis parameters are given in the legend. The slope was calculated with reduced major-axis linear regression (Hirsch and Gilroy, 1984). The dotted line represents the 1:1 relationship and the solid lines the 30% deviation range. (right) Seasonal mean tropospheric  $\text{NO}_2$  columns for December–February (DJF), March–May (MAM), June–August (JJA), and September–November (SON) for 2006–2011 from MAX-DOAS (open bars) and OMI (filled bars). The vertical lines are the standard deviation of the seasonal average.

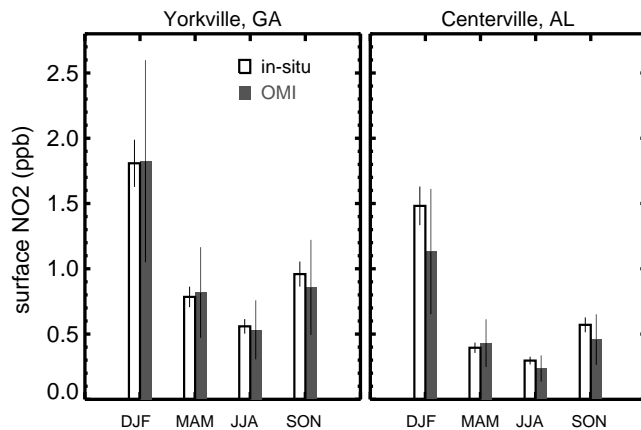


**Fig. 11.** Seasonal variation of  $\text{NO}_2$  mixing ratios at rural SEARCH sites for 2006–2010. Open bars represent seasonal mean  $\text{NO}_2$  mixing ratios from in situ measurements, and solid bars represent those derived from the OMI tropospheric  $\text{NO}_2$  columns. Error bars in in situ measurements represent 10% errors in the photolytic converter measurements. Error bars in the OMI-derived surface  $\text{NO}_2$  represent errors in retrievals including errors in the GEOS-Chem  $\text{NO}_2$  profiles.

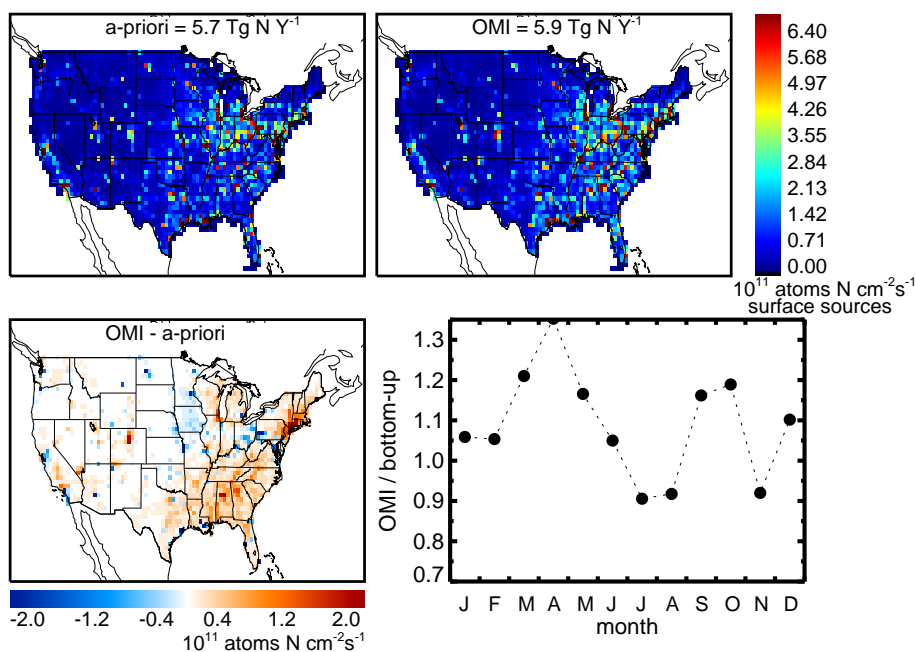


**Fig. 12.** (top) Annual mean surface  $\text{NO}_x$  emissions over the United States for 2005. The left panel contains bottom-up emissions from fossil fuels, bio-fuels, biomass burning, and soils. The right panel shows top-down emissions estimated using OMI tropospheric  $\text{NO}_2$  columns. The bottom left panel shows the difference between top-down and bottom-up surface  $\text{NO}_x$  emissions. (bottom right) Monthly mean ratio of area-averaged top-down surface  $\text{NO}_x$  emissions to bottom-up emissions over the United States.

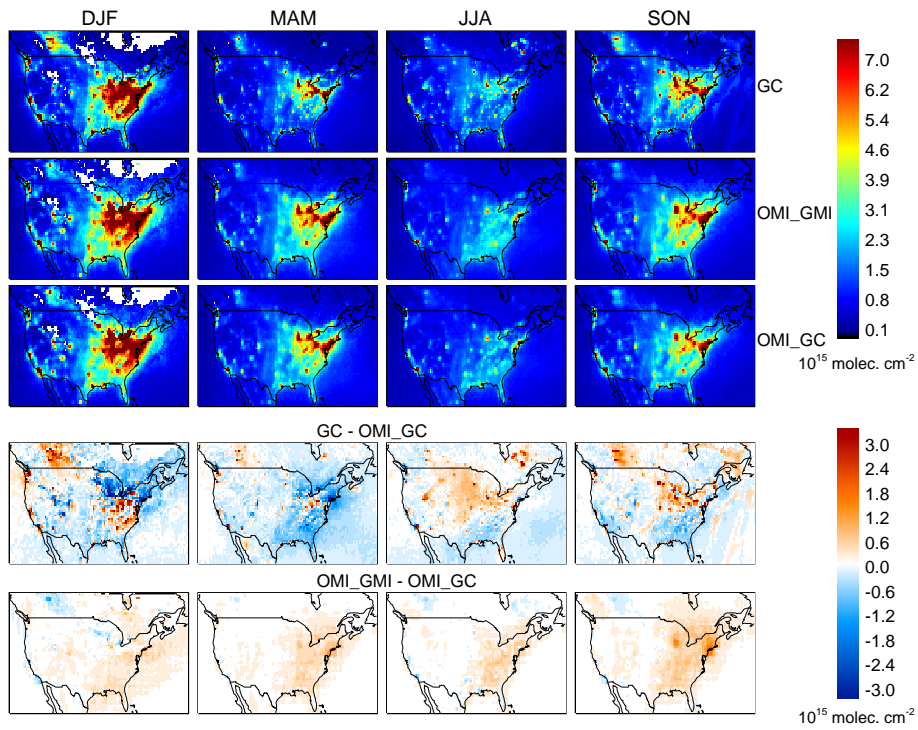


**Fig. 13.** Seasonal mean tropospheric NO<sub>2</sub> columns binned at  $0.5^\circ \times 0.667^\circ$  latitude  $\times$  longitude over North America for 2005 from GEOS-Chem (first row), OMI standard product (OMI.GMI, second row), and OMI retrievals using the GEOS-Chem NO<sub>2</sub> a priori vertical profiles (OMI\_GC, third row). White areas represent regions with insufficient data. The bottom two rows show the difference between (fourth row) GEOS-Chem and OMI\_GC, and (fifth row) OMI.GMI and OMI\_GC.